THE PROCEEDINGS OF
THE PHYSICAL SOCIETY

Section B

VOL. 62, PART 4 1 April 1949 No. 352 B

Measured Properties of Strong "Unipotential" Electron Lenses

BY G. LIEBMANN

Research Laboratory, Associated Electrical Industries Limited, Aldermaston, Berks.

MS. received 27th May 1948, and in amended form 18th October 1948; read at Science Meeting 3rd December 1948

ABSTRACT. The Hartmann test and the "knife-edge" method for the determination of lens constants are described as applied to the investigation of electrostatic "unipotential" lenses. The results of measurements on a number of such lenses are presented graphically.

It is shown that the curvature of the principal surfaces plays an important part and that it is, therefore, necessary to distinguish between longitudinal spherical aberration and difference of zonal focal lengths. Up to about half the lens diameter, primary spherical aberration only is noticeable in most cases. The dimensionless spherical aberration constant S can be approximately represented, over a wide range of modifications of lens design or lens potentials, by the formula $S=K_1(f/D)^2$, f being the focal length and D the internal diameter of the centre electrode of the lens. K_1 is a constant of the order of 10 for the lenses investigated without stops limiting the axial length of the field, and of the order of 20 for lenses incorporating such stops. In the case of one specially constructed lens, good agreement is found with calculations by Ramberg. In an experimental unipotential lens from which the diverging parts of the electrostatic field were removed, the spherical aberration is as low as in magnetic lenses of comparable dimensions.

§ 1. INTRODUCTION

THE "unipotential" or "single" lens occupies a unique position amongst the known electron lenses. It shares with the other electrostatic lenses the advantage that its properties are independent of the ratio e/m of charge to mass of the focused particle and depend only on the ratios of the lens dimensions and on the ratios of the voltages applied to its electrodes (provided that the particle speed is so low that no relativistic corrections are required). Its distinguishing feature is that its electrodes need only be connected to the cathode potential and to the final anode potential, which is mostly earthed. This simplifies the electrical circuits associated with the lens and makes the lens action largely independent of variations of the potential difference between cathode and anode.

The two basic forms of the "unipotential" lens are three perforated diaphragms with aligned circular holes, and a short cylinder placed between two longer cylinders. The outside electrodes are connected to the same potential, V_a, and the centre electrode to the cathode of the electron-optical system, or to any other suitable potential $V_c \neq V_a$. If $V_c \neq 0$, the advantages of making the lens action independent of the lens voltages is lost, but greater flexibility in operation is gained. If V_c is sufficiently negative, the lens is converted into an electron mirror.

The "unipotential" lens is used in cathode-ray tubes, in electrostatic electron microscopes, and in ion focusing devices. The image-forming electron bundles are here frequently of such angular aperture that the aberrations of the focusing lens may become of considerable importance. Spherical aberration in particular limits the performance of cathode-ray tubes (Maloff and Epstein 1938, p. 132) and of electron microscopes (Rebsch 1938). Whilst the theory of the "unipotential" lens has been discussed extensively (Scherzer 1933, 1936, Rebsch and Schneider 1937, Plass 1942, Ramberg 1942, Bachman and Ramo 1943, Bruck and Romani 1944, and others), little attention was given to the measurement of their properties except by Johannson and Scherzer (1933), Gobrecht (1941), and Mahl and Recknagel (1944).

Because of this lack of information, the writer studied experimentally several such lenses during 1942–1944, mainly to find out whether modifications of the basic design could give low spherical aberration values.

§ 2. GEOMETRIC-OPTICAL RELATIONS

For the "unipotential" lens, the refractive index of the medium is the same in image space and object space, and the lens formula can be written in the simple form

$$1/a+1/b=1/f, \qquad \ldots\ldots(1)$$

where a is the distance of the object P and b the distance of the image Q from their conjugate principal surfaces, and f is the focal length—see Figure 1, where the principal surfaces H and H′ are shown crossed-over and curved, as is found in actual measurements. All unipotential lenses investigated were of the symmetrical type; in this case the principal surfaces are symmetrical about the mid-plane M of the lens and intersect the optical axis at a distance $d_0/2$ from the mid-plane, d_0 being the separation of the apexes of the principal surfaces. The dimensions a, b and d_0 are not directly measurable; the values determined by the experiment are the object distance p and the image distance q from an arbitrary reference plane, e.g. mid-plane M, and the angles α and β of the rays in the object and image spaces.

If we let several rays from the object point P fall on the lens at different heights of incidence r_n (measured at R_n the point of intersection of ray and principal surface H), we find that the image points Q_n are displaced in an axial direction from the paraxial image point Q_0 towards the lens. The difference $q_0-q_n=\Delta q_n$ is the longitudinal spherical aberration. The nth ray cuts the plane perpendicular to the optical axis through the image point Q_0, the "Gaussian" image plane, at a distance δ_n from the axis. δ_n is the lateral spherical aberration (radius of the "disc of confusion" due to the nth lens zone).

It is customary to refer the aberrations to the focal plane, i.e. to consider the aberrations produced by a bundle of rays entering the lens parallel to the optical axis. The distance of the focus of the nth zone from the mid-plane will be denoted by q_n^*. From the theory of lens aberrations it is known that the primary longitudinal and primary lateral spherical aberrations of the nth zone can be written in this form (f_0 = paraxial focal length):

$$\Delta q_n^* = Sf_0(r_n/f_0)^2 \qquad \ldots\ldots(2)$$

and

$$\delta_n^* = Sf_0(r_n/f_0)^3. \qquad \ldots\ldots(3)$$

S is a dimensionless constant characterizing the spherical aberration of the lens (Bachman and Ramo 1943), dependent on the lens geometry and relative refracting

power, but independent of the lens dimensions. It is therefore particularly convenient in a comparison of the aberrations of various types of lenses; it is related to the frequently used aberration constant C_S (Cosslett 1945) by the formula

$$C_S = Sf_0.\dagger \qquad \ldots\ldots(4)$$

It is seen from equation (1) that for a finite object distance, as indicated in Figure 1, formulae (2) and (3) are replaced by $\Delta q_n = (b_0/f_0)(b_n/f_n)\Delta q_n^*$ and

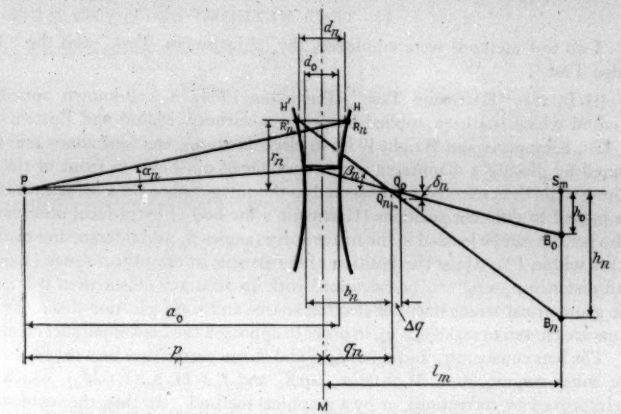

Figure 1. Diagram of optical paths through (thick) lens.

$\delta_n = (r_n/b_n)\Delta q_n$. Neglecting second-order terms, we obtain from these equations two alternative expressions for the constant S:

$$S = (\Delta q_n/r_n^2)(f_0^3/b_0^2), \qquad \ldots\ldots(5)$$

and

$$S = (\delta_n/b_0)(f_0/r_n)^3. \qquad \ldots\ldots(6)$$

An assumption, made by most authors, is that the principal surfaces are planes. The present measurements showed however that they are more nearly paraboloids.‡ Hence, a meridional section through each principal surface can be expressed in the form $\frac{1}{2}d_n = \frac{1}{2}d_0 - r_n^2(T-\frac{1}{2})/f_0$. The shift $\Delta d/2$ of the principal surface from its mid-plane distance $d_0/2$ on the axis is therefore given by the equation

$$\Delta d_n/2 = r_n(T-\tfrac{1}{2})/f_0. \qquad \ldots\ldots(7)$$

The dimensionless constant T is proportional to the *coma* of the lens. A value $T=0$ would represent a slight curvature of the principal surface such that, in the absence of spherical aberration, $S=0$, the lens would fulfil the "sine-condition" i.e. would give uniform magnification for off-axis points.

† Ramberg denotes the aberration constant S by C, Scherzer and others C_S by C_0.

‡ A curvature of the principal surfaces had already been observed in magnetic lenses (Becker and Wallraff 1938), but has not previously been found in electrostatic lenses.

If the focal length is measured, as usual in light optics, along the ray, we have for the zonal difference of focal length $\Delta f_n = f_n - f_0$ (provided $p_0 \gg f_0$): $\Delta f_n = \Delta q_n^* \doteq \frac{1}{2}\Delta d_n + r_n^2/2f_0$. Hence

$$\Delta f_n = r_n^2(S-T)/f_0, \qquad \ldots\ldots(8)$$

or

$$S = T + f_0 \Delta f_n / r_n^2. \qquad \ldots\ldots(9)$$

This zonal difference of focal length produces a zonal difference of magnification ΔM_n, as $M_n \simeq f_n/p_0$ for $p_0 \gg f_0$. ΔM_n is therefore proportional to $(S-T)$.

§ 3. TEST METHODS

Two test methods were employed, the "Hartmann Test" and the "Knife Edge Test".

(i) In the "Hartmann Test" (Hartmann 1904), a well-known optical test method which has been applied by previous authors (Maloff and Epstein 1938, p. 130, Klemperer and Wright 1939) to electron lenses, the lens zones are determined by placing a diaphragm with a number of pin-holes in front of the lens. The pencils thus selected are observed in the image space on a screen which can be moved to different positions (Hartmann's method of extra-focal observation). The pencils can be located in the image space (angles β_n and intersection distances q_n) to within 1%, whilst the position of the pencils in the object space (angles α_n and distance $p_n = p_0$) can be calculated with an accuracy closer than 0·3% from the geometrical arrangement of electron source and zone selection disc. Dimensions are chosen to make $p_0 \gg q_n$, in order to approach the case of parallel incidence.

The lens constants f_n and d_n, or f_0, S and T, can then either be worked out from the zonal magnification $M_n = \tan\alpha_n/\tan\beta_n$ and $f_n = M_n p_0/(1+M_n)$, which may be improved by corrections, or by a graphical method. In this, the incident and emergent rays are plotted on graph paper on a large scale, object point P and image points Q_n being placed on the same side of the lens. The incident ray is plotted above and the emergent ray below the optical axis. Figure 2 represents such a plot (lens No. 4)· The intersections of the conjugate rays then define the points R_n on the principal surface. Hence, $d_n/2$, q_n and δ_n can be taken from the graph. Then a_n and b_n are easily found, and f_n is obtained from the lens formula equation (1).

To find S and T, the fractions $\Delta q_n/r_n^2$, δ_n/r_n^3, $\frac{1}{2}d_n/r_n^2$, and $\Delta f_n/r_n^2$ are formed; their *average* values are then inserted into equations (5), (6), (7) and (9). Thus, each value of S and T is obtained from a number of measured points, giving a fairly reliable result. Agreement of the three values of S, determined from relations (5), (6) and (9), was usually within 10% or better. The S values given below are the averages of these three evaluations.

The accuracy of the final values of f_0 is estimated as closer than $\pm 1\%$, of S about $\pm 10\%$, and of $d_0/2$ and T about $\pm 20\%$.

(ii) In the "Knife Edge" method the aberration is determined from the distortion of a straight edge, e.g. the edge of a narrow slit (see also Boersch 1939, Dosse 1941). It is particularly applicable to lenses which show little aberration, or when it is desirable to observe only for small angular apertures α and β. It was, however, not recognized by the earlier authors that the test as described by them did not give S but $(S-T)$ and was, therefore, not a true test of spherical aberration; only in bad lenses, as we shall see later, is S so much greater than T that $(S-T)$ can be considered as nearly equal to S.

If we place a "knife edge" a distance y from the axis (Figure 3) and illuminate it with a bundle of rays originating in P, we should, in the absence of spherical aberration, obtain a "shadowgraph" of the knife edge at the position B_0 on the screen, located at a distance l from the mid-plane M of the lens.

As the ray after leaving the lens does not pass through the paraxial image point Q_0 but through the zonal image point Q_1 corresponding to the zone distance r_1 from the axis (r_1 being the off-axis distance of point R_1, the projection of the knife edge on to the principal surface H from the point P), the "shadowgraph" will be displaced to the point B_1.

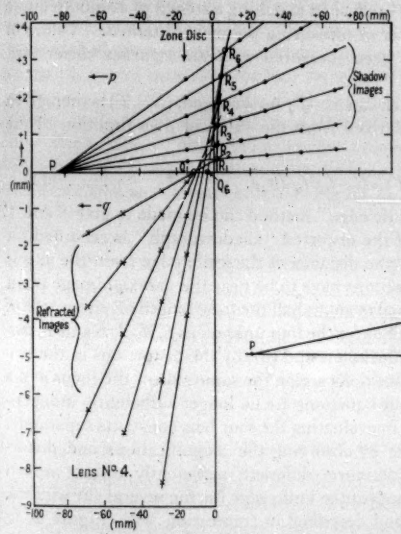

Figure 2. Experimental plot of electron pencils through lens under test.

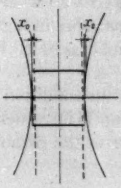

Figure 4.

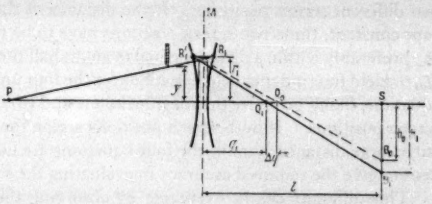

Figure 3.

Figure 3. Diagram of "knife-edge" test.
Figure 4. Determination of displacement x_0 of apex of parabola in "knife-edge" test.

From the geometrical relations of Figure 3 it can be derived (see Appendix I) that the displacement $\Delta h = h_1 - h_0$ of the point Q_1 from point Q_0 is given, for $\Delta f/f_0 \ll 1$, by $\Delta h = l r_1 \Delta f / f_0^2$.

In view of equation (8), this can be written as

$$\Delta h = l(r_1/f_0)^3(S-T). \qquad \ldots\ldots(10)$$

The shadow image of the straight "knife edge" will therefore appear curved, showing as a rule pincushion distortion. It can be proved from the cubic law of primary spherical aberration that the distorted image of the edge is a parabola, the origin of which is displaced by the amount $x_0 = l(S-T)(r_1/f_0)^3$, the same value as given by equation (10). If the "knife edge" forms the edge of a slit placed symmetrically about the axis and a square is inscribed into the centre part of the "shadowgraph" image of the slit (see Figure 4), then the displacement of the image measured along the sides of the square equals $2x_0$. Hence the required

displacement x_0 of the apex of the parabola can be easily obtained as the difference of the half-width of the square and the half-width of the "waist" of the shadow image; $(S-T)$ is then found from equation (10). f_0 can be determined from the angular magnification as discussed before, and l and r_1 are given by the geometry of the test arrangement.

The accuracy of measuring $(S-T)$ by this method can be greatly increased if the radius of curvature ρ of the parabola is used as a measure of the distortion. This can be done by placing stencils (e.g. circles drawn on a sheet of celluloid) on a photograph of the distorted shadow image of the "knife edge". This method of measuring $(S-T)$ is very accurate because in matching a stencil to a smooth curve the *average* value of a great number of measuring points is obtained. Values of $\Delta f/f_0$ as small as 0·01 have thus been measured with an accuracy closer than $\pm 10\%$.

Under the condition $p \gg f_0$, which can usually be arranged, $(S-T)$ is then given by equation (11), which can be derived from the value of ρ as function of the parameters of the parabola:

$$(S-T)=(l-f_0)^2 f_0/2lr_1\rho. \qquad \ldots\ldots(11)$$

It should be noted that the "knife edge" method can be made to give S and T separately as well as f_0 and $d_0/2$, if the distorted "shadowgraph" is recorded for two different screen positions. If the distance of the knife edge from the axis is kept constant, these two screen positions have to be near the paraxial image point Q_0, preferably within a distance equal to about half the focal length on either side of Q_0, to yield four independent equations for the four unknowns f_0, $d_0/2$, S and T, two equations being given by the magnifications and two by the distortions in the two screen positions. If both screen positions are on the same side of the focus and a fairly large distance from it, the four equations are no longer sufficiently independent to give the required accuracy in evaluating the four lens constants separately.

This difficulty can be overcome by observing the magnifications and distortions of the knife edge for two (or more) different, sufficiently distant screen positions for several off-axis distances of the knife edge (or for several slit widths), and then using the graphical method described in connection with Figure 2, in conjunction with the $(S-T)$ values obtained from the distortion measurements.

These conditions were only fully recognized after the experimental work described in this paper was completed. As a constant slit width was used, only f_0, $d_0/2$, and $(S-T)$ were measured.

§ 4. EXPERIMENTAL TECHNIQUE

Most lenses investigated were built up from equal diameter tubular elements, and were constructed as parts of small sealed-off cathode-ray tubes.

The construction of such a "lens-test tube" is shown diagrammatically in Figure 5. The electron beam was produced by a triode electron gun of conventional type. The anodes A_1 and A_2, forming the outer elements of the unipotential lens L, and its centre electrode A_c were made from $\frac{1}{2}$ in. diameter seamless non-magnetic nickel copper alloy tubing (bore $D=11{\cdot}7$ mm.). The electrodes were mounted in the usual way on mica discs held rigidly in position by four stout non-magnetic alloy rods. These rods extended about 4 in. beyond the end of the electrode A_2 and served as guide rods for the sliding fluorescent screen S. The

whole assembly was mounted on a stem F and sealed into a tubular internally "metallized" envelope E, the end part of which consisted of a light walled bulb free from optical imperfections.

A "zone disc" Z (or a parallel edged slit when the knife-edge method was used) was arranged, as a rule, in a field-free position within the anode cylinder A_1. Six pairs of holes at different off-axis distances were drilled in the zone disc, allowing the simultaneous observation of six zones. The positions of the holes of each zone disc were carefully measured with a projecting microscope.

The fluorescent screen could be moved by tapping the tube. The screen position could be read on a scale fixed to the outside of the tube envelope. The image of the electron pencils on the fluorescent screen was photographed in a 1 : 1 ratio, and all measurements were taken on the photographic plate. The positions of the rays were measured for four screen positions, moving the screen from one extreme end to the other. To check the correctness of the scale readings of the screen positions, photographs were taken as well of the "shadow images" of the zone disc or slit. These shadow images were obtained as the straight line projections from the point P of the holes in the zone disc when V_c was made equal to V_a, i.e. if the lens action was removed (Figure 2).

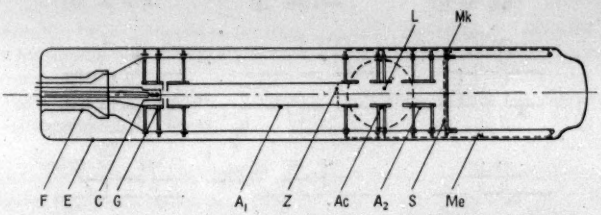

Figure 5. Experimental "lens test" cathode-ray tube.

The influence of the field of the four supporting rods which penetrates through the gaps between the centre electrode of the lens and its outer electrodes was found negligible in all but the largest lens zone used, becoming just detectable in the outermost zone ($r_6 \simeq D/4$).

§ 5. LENS TYPES INVESTIGATED

Fourteen different unipotential lenses were investigated. The essential design parameters measured in lens diameters D, except for lenses Nos. 13 and 14, where the dimensions are given in millimetres, are shown diagrammatically in Figure 6.

The lenses Nos. 1 to 6 are of the same type and may be arranged in ascending order of lens thickness, although a lengthening of the centre electrode, leaving the gaps between electrodes unchanged, is more effective in thickening the lens than leaving the centre electrode unchanged and lengthening the gaps. The relative order of lenses Nos. 4 and 5 might therefore be reversed.

Lens No. 7 is similar in dimensions to lens No. 3, but contains two diaphragms across the outer electrodes of the lens, each provided with a centre hole. This lens was made to study the influence of the holes in the diaphragms on the spherical aberration. As it appeared that the field near these holes was still rather high,

lens No. 8 was constructed; this is similar to lens No. 7, but has the diaphragms removed further into the outer electrodes, thus placing them into a rather weaker field.

Lens No. 9 was made in order to study the properties of an electrostatic lens from which the diverging field sections have been removed. It is identical in dimensions with lens No. 7, but the diaphragms are replaced by the zone disc on one side and by an open wire mesh disc (120 meshes per inch, about 70% transparency) on the other side. Although each hole in the zone disc acts as a lens, the

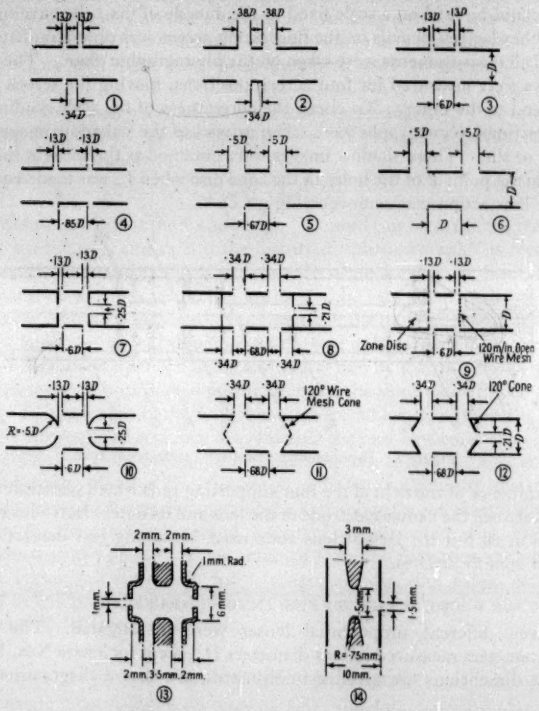

Figure 6. Types of investigated lenses.

principal ray passing through the centre of the hole is not deflected from its position, and the effect of such "pinhole lens" is only a decrease or increase in the size of the cross-section of the electron bundles which pass through it and enter the main lens.* A similar argument can be applied to the section of the wire mesh. The field shape in this lens is such that it is purely converging, whereas all other unipotential lenses have diverging fields at the entrance to, and exit from, the lens.

* This point has since been discussed more fully by Gabor in connection with ion-focusing grids (Gabor 1947).

Hence lens No. 9 has rather interesting properties, although it is not a practical proposition as a focusing element in ordinary applications. Further, this lens allows a clear-cut comparison with lens No. 7, being only different from this by the absence of the entrance and exit holes.

Lens No. 10 also is almost identical with lens No. 7, but the ends of the outer lens electrodes which face the centre electrode are hemispherically curved, in an attempt to change, at least in part, the curvature of the equipotential field surfaces near the outer lens electrodes in a more favourable direction.

Lenses No. 11 and 12 as well are similar to lens No. 7, but incorporate conical inserts (cone angle 120°) which serve to reduce the field where the entrance and exit apertures are situated. The only difference between these two lenses is the presence of apertures in lens No. 12.

Lens No. 13 is similar to lens No. 8, except for a rounding-off of the edges of the electrodes. It was used as objective lens in an experimental three-stage electrostatic electron microscope constructed by the writer some years ago. This lens is not the best one tested from the point of view of spherical aberration, but was chosen because it appeared to lend itself to comparatively easy manufacture and easy alignment, and because it showed a quick decay of the electric field outside the lens.

Lens No. 14 corresponds to the lens "Type B" described and analysed in its action by Ramberg (1942), and was made in order to see how closely theory and experiment would agree.

Lenses Nos. 13 and 14 were tested by the knife-edge method, all others by the Hartmann method.

§ 6. TEST RESULTS

The measured lens constants as functions of relative zone radius r/D are plotted in Figures 7 and 8 for lenses Nos. 1 to 12, all for the condition $V_c/V_a = 0$. These figures give the relative focal length f/D, the relative focal distance q^*/D from the mid-plane of the lens, and the relative distance $\frac{1}{2}d/D$ of the principal surface from the mid-plane for rays of parallel incidence. It can be seen how necessary it is to distinguish between longitudinal spherical aberration $\Delta q_n = (q_0^* - q_n^*)$ and zonal difference in focal length $\Delta f_n = (f_0 - f_n)$.

In Figure 7 we see that a progressive increase in the lens thickness leads to an increase in refracting power; the longitudinal spherical aberration decreases in step with the paraxial focal length f_0, so that $\Delta f/f_0$ or $\Delta q/q_0$ remain almost constant, for a given off-axis distance r/D. The parameter T remains practically constant within measuring accuracy, at a value around 6.

This picture changes when we come to the very thick lenses, Nos. 5 and 6. The paraxial focal length of these lenses has not decreased further, and the curvature of the principal surfaces has increased instead, becoming very great for lens No. 6, the parameter T rising to 10 in lens No. 5 and to 14 in lens No. 6. The rise in T is, indeed, so pronounced that the spherical aberration constant S, which showed a decrease with increasing lens strength in the first lenses, rises sharply, although the term $(S - T)$ shows a slight further drop. Lens No. 6 is particularly interesting; the zonal focal length, which decreases for small off-axis distances, increases again for greater distances, becoming equal to the paraxial focal length f_0 at a distance $r_0/D = 0{\cdot}2$, even increasing beyond the paraxial value for greater values of r/D. Thus the curve of f/D resembles the familiar aberration curves of spherically corrected optical systems. Nevertheless, lens No. 6 shows a high degree of

spherical aberration, given by the q^*/D curve, as the principal surfaces recede much more quickly from the mid-plane of the lens for increasing off-axis distances than the zonal focal length increases; the shape of the f/D curve is mainly due to the fact that the paraxial focus lies within the lens field. This behaviour of electron lenses for large off-axis distances, which was found to a lesser degree also in some

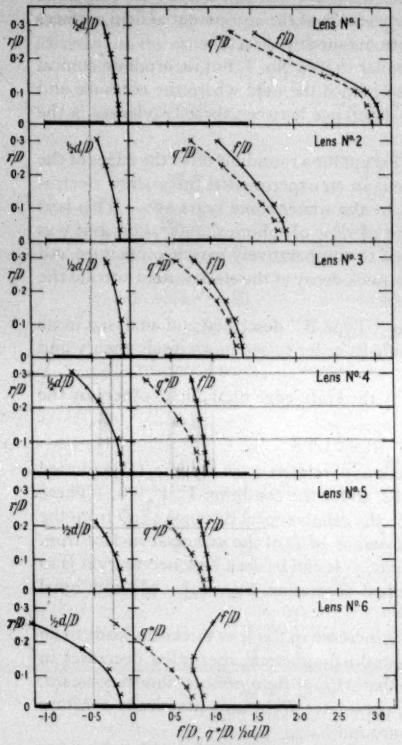

Figure 7. Relative focal length f/D, relative focal distance (for rays incident parallel to optical axis) q^*/D, and relative separation of principal surfaces from mid-plane of lens $\frac{1}{2}d/D$ as function of relative off-axis distance r/D for lenses Nos. 1–6.

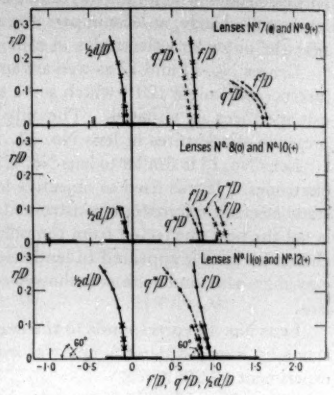

Figure 8.

Figure 9.

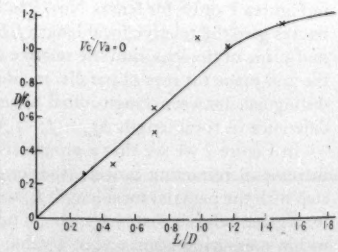

Figure 8. Relative focal length f/D, relative focal distance (for rays incident parallel to optical axis) q^*/D, and relative separation of principal surfaces from mid-plane of lens $\frac{1}{2}d/D$ as function of relative off-axis distance r/D for lenses Nos. 7–12.

Figure 9. Paraxial refractive power D/f_0 of lenses Nos. 1–6 as function of approximate length of lens L/D.

other cases (see for instance lens No. 1, Figure 7, and lens No. 12, Figure 8), may suggest a possibility of obtaining zonal correction. Mr. T. Mulvey pointed out to the writer that a lens such as No. 6 might be used with advantage as a partly distortion-free projector lens in electron microscopes.

In Figure 9 the relative refracting power D/f_0 for lenses Nos. 1–6 is plotted as a function of lens thickness L. Whilst the lens thickness would be more correctly defined as the length over which the electrostatic field exceeds a certain minimum value, it was taken here, for practical reasons, as the distance between the planes bisecting the gaps between inner and outer lens electrodes. This definition, which does not take full account of the actual length of the refracting field, is probably the main reason for the scatter of the points in Figure 9. The refracting power D/f_0 appears at first to go up in proportion to the lens thickness L, as one would expect from the formulae for the focal length of a weak electron lens, but seems to approach a maximum value of the order 1·2 to 1·5 (for $V_c=0$).

Turning now to lens No. 7, we see that the effect of the perforated diaphragms is a slight weakening of the refracting power (by 19%), whereas the spherical aberration constant S shows an increase by a factor of 2·8. The influence of the entrance and exit holes on the performance of the lens is thus very marked, contrary to the expectations of earlier authors (Bachman and Ramo 1943). This deterioration of performance is not altogether surprising owing to the addition theorem of the spherical aberrations of several lenses (see Appendix II), and the fact that the *relative* off-axis distance used by the electron beam passing through the entrance and exit holes is very much greater than in the main lens.

Lens No. 8 shows a rather small relative focal length, indicating that the removal of the entrance and exit holes into regions of a weak field has been effective in eliminating the influence of these holes on the focal length; yet the increase of the spherical aberration over that of lenses without diaphragms is still appreciable.

The properties of lens No. 10 fall half way between those of lenses Nos. 7 and 8, as might be expected from its geometry.

A comparison of lenses Nos. 11 and 12, which are similar to lens No. 8 in dimensions and optical constants, brings out once more very clearly the influence of apertures not situated in an absolutely field-free region. The paraxial focal length remains unaffected but the spherical aberration is doubled.

We find a reverse effect in lens No. 9. The elimination of the diverging parts of the lens field leads to a decrease in focal length and to a considerable improvement in spherical aberration, putting this lens into a class of its own amongst the electrostatic lenses investigated. The spherical aberration constant of this lens is very nearly the same as that of a magnetic lens of the same f_0/D ratio.

A summary of the measured lens constants is given in the Table. To bring out further the connection between focal length and spherical aberration and coma, the values of the aberration constants S and $(S-T)$ are plotted in Figures 10 and 11 as functions of relative focal length f_0/D. Figure 10 indicates that for lenses whose basic design elements are cylinders the parameter S can be written as *

$$S=K_1(f_0/D)^2. \qquad \ldots\ldots(12)$$

The remarkable point is that the constant K_1 does not appear to depend, within wide limits, on the dimensions or even the shape of the lens elements, yet it is quite sensitive to the introduction of entrance and exit stops, as seen from the difference of the two curves in Figure 10. The very thick lenses Nos. 5 and 6 are omitted since they do not fall on the curve, the constant S being rather higher. In contrast to this, lens No. 9, the purely converging lens, has an aberration constant

* Lenses whose elements are diaphragms do not seem to follow such simple law.

which is smaller by a factor of about 2·5 than would be expected from the lower curve in Figure 10. The constant K_1 has a value of 9·5 for the lower curve, and a value of 18 for the upper curve.

In Figure 11, the parameter $(S-T)$ is plotted for all lenses except No. 14. Apart from the very thick lenses, for which $(S-T)$ falls away more quickly, the parameter $(S-T)$ can be represented by the formula

$$(S-T)=K_2(f_0/D)^{2\cdot5}. \qquad \ldots\ldots(13)$$

Again the constant K_2 is about twice as great for lenses with entrance and exit stops as for the others, being about 10 for the former and about 5 for the latter.

Table

Lens No.	V_c/V_a	f_0/D (±1%)	$\frac{1}{2}d_0/D$ (±20%)	S (±10%)	T (±20%)	$S-T$ (±25%)	Remarks
1	0	3·10	0·11	91	6·0	85	
2	0	1·92	0·10	35	6·3	29	
3	0	1·39	0·09	16·5	4·8	11·7	
4	0	0·92	0·09	9·0	6·0	3·0	
5	0	0·97	0·09	12·5	10·0	2·5	
6	0	0·86	0·11	17·0	14·0	3·0	
7	0	1·65	0·04	46	7·4	39	Diaphragms
8	0	0·87	0·04	14·2	6·6	7·6	Diaphragms
9	0	0·78	0·09	2·6	2·0	0·6	Converging only
10	0	1·15	0·06	23·5	10·0	13·5	Diaphragms
11	0	0·93	0·09	7·5	3·8	3·7	Conical inserts
12	0	0·93	0·09	12·0	3·6	8·4 (±10%)	As No. 11 but diaphragms
13	+0·20	2·43	(0·11)	—	—	77	Similar to No. 8 but rounded electrodes
	+0·10	1·70	(0·11)	—	—	30	
	0	1·22	0·11	—	—	10·5	
	−0·10	0·83	(0·11)	—	—	4·7	
	−0·20	3·58	(0·11)	—	—	1·9	
14	+0·30	4·38	0·12	—	—	72	Ramberg's " B " lens
	+0·20	2·82	0·12	—	—	29·5	
	+0·10	2·02	0·12	—	—	15·5	
	0	1·38	0·12	—	—	8·4	
	−0·10	0·94	0·12	—	—	5·2	

The full circles (intermediate curve) refer to lens No. 13, for which only $(S-T)$ could be measured, the different values of f_0/D being produced by changing the ratio V_c/V_a of the electrode voltages. From this we conclude that, within wide limits, the aberration parameter $(S-T)$ depends mainly on the relative focal length f_0/D, whether this be brought about by a change in design or by an adjustment of electrode potentials, the values of S or $(S-T)$ in different types of the investigated lenses not varying by more than a factor of two except in extreme cases.

A comparison of theory and experiment are given by Figure 12, where the refracting power D/f_0 and the parameter $(S-T)D^2/f^2$ are plotted for lens No. 14 (Ramberg's " B " lens) as a function of $\{(V_a-V_c)/V_a\}^{\frac{1}{2}}$. It has to be remembered that Ramberg's calculated ζ/M value is not $(S-T)D^2/f_0^2$ but SD^2/f_0^2. Nevertheless, the agreement between Ramberg's calculations and these measurements is very satisfactory, the constant T probably being rather small in this case. This lens is

indeed better for a given f_0/D value than the other lenses measured (except lens No. 9), but the difference is small, and still within a factor of two.

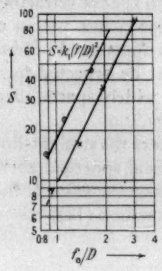

Figure 10. Spherical aberration constant S as function of relative paraxial focal length f_0/D. ×, lenses Nos. 1–4; ○, lenses Nos. 7, 8 and 10.

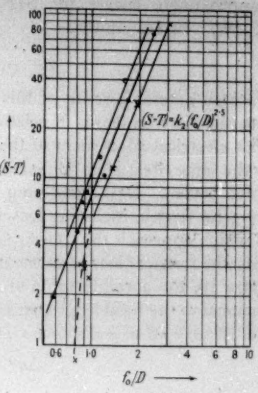

Figure 11. Aberration term $(S-T)$ as function of relative paraxial focal length f_0/D for lenses Nos. 1–13.

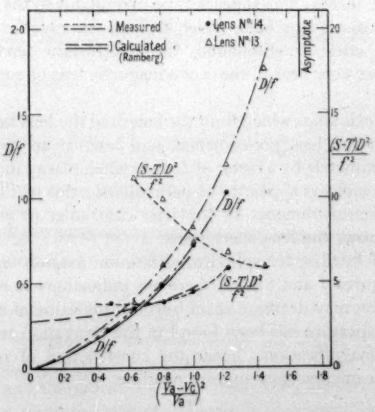

Figure 12. Refractive power D/f and aberration constant $(S-T)D^2/f^2$ as function of centre electrode potential $(V_a-V_c)^2/V_a^2$, as measured for lenses Nos. 13 and 14, and as calculated by Ramberg for lens No. 14.

Figure 12 also gives the measurements on lens No. 13 plotted in the same way. At low refracting powers this lens is appreciably worse than Ramberg's lens, but approaches this closely at high refracting powers.

The influence of the T term would be most noticeable for the lower $(S-T)$ values; as the length of a lens does not change with a change of electrode potentials, it is reasonable to assume that the values of T will not show very great changes, and that approximate curves for SD^2/f_0^2 would be obtained by displacing the $(S-T)D^2/f^2$ curves upwards.

§7. CONCLUSION

We may note as a result of this investigation that the main parameter of a unipotential electron lens is its relative focal length f_0/D or refracting power D/f_0, and that electrical adjustment of the refractive power has, within certain limits, nearly the same effect as an adjustment of the lens dimensions producing the same refractive power. Deviations from this rule may be expected for lenses of unusually great length, including lenses formed by widely spaced diaphragms, and lenses which approach the "electron mirror" condition.

Over the range of lens adjustments which follows the straight-line relationship of Figure 10, the absolute value of the longitudinal spherical aberration Δq^* is proportional to the focal length, and only depends on the value of the constant K_1 and the relative off-axis distance r/D, as (from equation (12))

$$\Delta q^* = K_1 f_0 (r/D)^2, \qquad \ldots\ldots(14)$$

the constant K_1 being of the order of 8 to 20. Hence the larger the lens diameter, for a given *focal length*, the better the lens.†

Electrostatic lenses of the type investigated have spherical aberration constants S which are approximately three to four times greater than those of corresponding magnetic lenses; this appears to be mainly due to the diverging effect of parts of the electrostatic lens field, which deflects the rays further from the axis. If the diverging effect is eliminated, the electrostatic lens yields aberration constants which are very near to those of a magnetic lens of comparable refracting power.

Entrance and exit stops which limit the length of the lens field have a considerable influence on the lens performance, and lead to an increase in spherical aberration, approximately by a factor of 2, even when placed in a weak field region.

The principal surfaces appear to be paraboloids; this fact has to be taken into consideration in measurements of the lens constants, or in using simplified formulae representing the lens aberrations.

The region of third-order spherical aberration extends in most cases up to $r/D \simeq 0{\cdot}2$ (see Figures 7 and 8), but there are indications in some cases that the spherical aberration may decrease again beyond this value of r/D. An improvement with wider aperture has been found in the aberration term controlling the zonal change of magnification; hence the construction of improved projector lenses for electron microscopes appears possible.

ACKNOWLEDGMENTS

The experimental part of the work reported here was carried out by the writer whilst on the staff of Messrs. Cathodeon Ltd., whose Directors he wishes to thank for permission to publish these results. He further expresses his thanks to Dr. T. E. Allibone for allowing the completion and publication of the analysis of the experimental work.

† The larger lens diameter explains therefore, amongst other factors, the superiority of the magnetic lens over electrostatic lenses in cathode-ray tube focusing.

APPENDIX

I. *The "Knife-Edge" Test*

From the geometry of Figure 3 we have for the displacement of the shadow image of the straight edge

$$\Delta h = h_1 - h_0 = r\left[\frac{l-q_1}{b_1} - \frac{l-q_0}{b_0}\right],$$

with $b_0 = q_0 + \frac{1}{2}d_0$ and $b_1 = Q_1R_1' \simeq (q_0 + \frac{1}{2}d_0) - (\Delta q - \frac{1}{2}\Delta d) + r_n^2/2q_0$. This leads, for the screen distance l_j, to

$$\Delta h_j = \frac{r_n[\Delta q_n(l_j + \frac{1}{2}d_0) - (l_j - q_0)(\frac{1}{2}\Delta d + \frac{1}{2}r_n^2/2q_0)]}{(q_0 + \frac{1}{2}d_0)(q_0 + \frac{1}{2}d_0 - \Delta q_n + \frac{1}{2}\Delta d_n + r_n^2/2q_0)}. \quad \ldots\ldots(15)$$

Further, the magnification M_j at the screen in the position l_j is

$$M_j = (l_j - q_0)/(q_0 + \tfrac{1}{2}d_0). \quad \ldots\ldots(16)$$

Hence for $j = 1, 2$, i.e. two screen positions of which at least one fulfils the condition $l_j \gg q_0$, we have four independent equations for the unknowns q_0, Δq, $\frac{1}{2}d_0$, $\frac{1}{2}\Delta d$, from which f_0, S and T can be determined.

For $l \gg q_0$, equation (15) yields $\Delta h_n \simeq r_n l[\Delta q_n - (\frac{1}{2}\Delta d_n + r_n^2/2q_0)]/b_0^2$, which gives, with $\Delta q_n = r_n^2 S/f_0$ and $\frac{1}{2}\Delta d_n + r_n^2/2q_0 = r_n^2 T/f_0$, for $q_0 \simeq b_0 \simeq f_0$:

$$\Delta h_n = (r_n/f_0)^3 l(S-T). \quad \ldots\ldots(17)$$

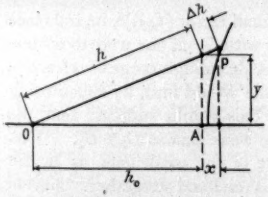

Figure 13. Diagram of distortion figure obtained in "knife-edge" test.

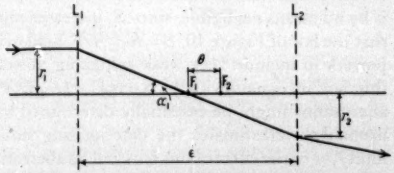

Figure 14. Optical path through system of two separated lenses.

From Figure 13 we have, taking the centre of the undistorted image of the straight edge as origin A for our coordinates x and y and neglecting the term $\Delta h/h_0$ in $(1 + \Delta h/h_0)$, $\Delta h \simeq hx/h_0$ and $y^2 = h^2 - h_0^2$. But from Figure 3 $h \simeq r(l - q_0)/f_0$. Eliminating Δh and h, we obtain the equation of a parabola :

$$y^2 = \frac{(l-q_0)^3}{lh_0(S-T)}x - h_0^2. \quad \ldots\ldots(18)$$

The apex of this parabola is displaced from the origin A by the amount $x_0 = h_0^3 l(S-T)/(l-q_0)^3$. For $y = h_0$ we obtain $x = 2x_0$; this is the basis of the rule for determining x_0 and therefore $(S-T)$ by measuring across the "waist" of the distorted image and along the side of the inscribed square (Figure 5).

The radius ρ of the osculating circle at the apex is one half the coefficient of x in the equation for y^2; hence

$$(S-T) = \frac{(l-q_0)^3}{2lh_0\rho} = \left(\frac{f_0}{r}\right)^3 \frac{h_0^2}{2l\rho}. \quad \ldots\ldots(19)$$

II. *Addition of Spherical Aberrations of Two Lenses*

Consider two lenses of focal lengths f_1 and f_2 and spherical aberration constants S_1 and S_2, a distance ϵ apart (Figure 14). The focal length of the combination is

then given by $f=f_1f_2/\theta$, where $\theta=f_1+f_2-\epsilon$. From $S=\Delta q^*f_0/r^2=\Delta qf/r^2$ we have $r=(\Delta qf/S)^{\frac{1}{2}}$. From Figure 14 we see that

$$\tan\alpha_1=\frac{r_1}{f_1}=\left(\frac{\Delta q_1}{S_1f_1}\right)^{\frac{1}{2}}=\frac{r_2}{f_2-\theta}=\left(\frac{\Delta q_2f_2}{S_2}\right)^{\frac{1}{2}}\frac{1}{f_2-\theta},$$

and

$$\Delta q_2/\Delta q_1=(f_2-\theta)^2S_2/f_1f_2S_1. \qquad \ldots\ldots(20)$$

The spherical aberration constant S of the combined lens system is then $S=\Delta qf/r_1^2=\Delta qfS_1/\Delta q_1f_1$. But the longitudinal spherical aberration Δq is the difference between paraxial focal length f and the focal distance of the ray of incidence height r_1; hence

$$\Delta q=\frac{f_1f_2}{\theta}-\frac{(f_1-\Delta q_1)(f_2-\Delta q_2)}{\theta+\Delta q_1+\Delta q_2}.$$

For rays not too far from the axis $\Delta q_1\ll\theta$; $\Delta q_2\ll\theta$ hence $\Delta q\simeq(\Delta q_1f_2+\Delta q_2f_1)/\theta$. Substituting the constants S in place of the Δq's, and using equation (20), we find

$$S=\{f_2^2S_1+(\epsilon-f_1)^2S_2\}/\theta^2. \qquad \ldots\ldots(21)$$

If one lens is a very weak lens, $f_1\gg f_2$, the expression simplifies to

$$S=(f_2/f_1)^2S_1+S_2. \qquad \ldots\ldots(22)$$

Hence the aberration of the combined system is always greater than that of the individual lenses unless the signs of S_1 and S_2 are different, a case not normally encountered in electron optics.

Although the constant S_1 is multiplied by the small factor $(f_2/f_1)^2$, its influence is by no means negligible, since S_1 increases rapidly with f. If one were to assume that the law of Figure 10, $S=K_1(f/D)^3$, held over a wide enough range of refractive powers to include very weak refracting powers, one would find, by substituting this law in equation (22), $S=S_2[1+(D_2/D_1)^3]$. This would indicate that the aberrations might be essentially determined by the weak lens as $D_2\gg D_1$. This probably overestimates the deteriorating influence of the weak lens, as in the limit $f_1\to\infty$ the effect of this lens and its aberrations is removed altogether. Nevertheless, we should still expect an appreciable contribution by the weak lens to the spherical aberration of the lens combination even when its contribution to the refracting power is quite negligible.

REFERENCES

Bachman, C. H., and Ramo, S., 1943, *J. Appl. Phys.*, **14**, 8.
Becker, H., and Wallraff, A., 1938, *Arch. Elektrotech.*, **32**, 664.
Boersch, H., 1939, *Z. tech. Phys.*, **20**, 346.
Bruck, H., and Romani, L., 1944, *Cahiers de Physique*, No. 24, 15.
Cosslett, V. E., 1945, *J. Sci. Instrum.*, **22**, 170.
Dosse, J., 1941, *Z. Phys.*, **117**, 722.
Gabor, D., 1947, *Nature, Lond.*, **159**, 303.
Gobrecht, R., 1941, *Arch. Elektrotech.*, **35**, 672.
Hartmann, J., 1904, *Z. Instrumkde*, **24**, 1.
Johannson, H., and Scherzer, O., 1933, *Z. Phys.*, **50**, 183.
Klemperer, O., and Wright, W. D., 1939, *Proc. Phys. Soc.*, **51**, 296.
Mahl, H., and Recknagel, A., 1944, *Z. Phys.*, **122**, 660.
Maloff, I. G., and Epstein, D. W., 1938, *Electron Optics in Television* (New York: McGraw-Hill Book Co.).
Plass, G. N., 1942, *J. Appl. Phys.*, **13**, 49.
Ramberg, E. G., 1942, *J. Appl. Phys.*, **13**, 582.
Rebsch, R., 1938, *Ann. Phys., Lpz.*, **31**, 551.
Rebsch, R., and Schneider, W., 1937, *Z. Phys.*, **107**, 138.
Scherzer, O., 1933, *Z. Phys.*, **80**, 193; 1936, *Ibid.*, **101**, 23, 593.

On the Electrical Properties of Cold Worked Iron Carbon Alloys

By A. B. BHATIA
H. H. Wills Physical Laboratory, University of Bristol *

Communicated by N. F. Mott; MS. received 21st August 1948

ABSTRACT. The change on "aging" in the electrical properties of cold worked iron–carbon alloys of low concentration is investigated theoretically. During the process of "aging", the carbon atoms diffuse into the dislocations, thus forming rows of atoms. The electrical resistance due to scattering of electrons *by these rows of carbon atoms* is expressed in terms of the scattering power of a single carbon atom dissolved in the iron lattice, and hence in terms of the resistance of the same number of randomly distributed carbon atoms. It is found that this change depends on the wavelength of the electrons at the Fermi surface. This wavelength is determined by the effective number of free electrons, and with a reasonable value of about 0·6 electrons per atom for iron, the agreement with the observed diminution in resistance is satisfactory.

Alternatively, one can use the calculations to determine both the number of free electrons in iron and the number of dislocations in the specimen at different degrees of hardening, from the observed changes in the electrical resistance and thermoelectric power of the specimen.

§1. INTRODUCTION

It is known that cold worked iron of low carbon content changes its mechanical and physical properties on "aging" at room temperature. For example, the critical shear strength for the material increases with time while its electrical resistance decreases. It has been suggested by Cottrell and Bilby (1949) that carbon atoms diffuse into regions of the lattice where it is slightly expanded by the presence of a dislocation, so as to make the elastic strain energy of the dislocation a minimum. They estimate from this the number of carbon atoms migrating into a dislocation as roughly one to two per atomic plane. This means (see §2) that the carbon atoms tend to rearrange themselves into rows parallel to the lines of dislocations.† It is the purpose of this paper to investigate theoretically the change in electrical resistance and thermoelectric power of these alloys, due to such a rearrangement of carbon atoms in them.

§2. PROBABLE DISTRIBUTION OF CARBON ATOMS IN DISLOCATIONS

The model of a dislocation used by Cottrell and Bilby in estimating the number of carbon atoms diffusing into it is shown in Figure 1. In the figure, the x-axis is the direction of glide, and the dislocation is assumed to extend along the z axis (perpendicular to the plane of the paper) throughout the entire length of the crystal. The slip plane according to the figure is the x–z plane. It should be noticed that each row above the x axis contains one more atom than the row below it.

Using the fact that the strain due to such a dislocation varies inversely with distance from the centre, Cottrell and Bilby deduce the *extra* density of carbon

* Now at Theoretical Physics Department, University of Liverpool.

† The author's thanks are due to Dr. A. H. Cottrell for supplying the results described in §§ 1 and 2 in a private communication.

atoms at any point (r, α) in the lower half of the plane as $K \sin\alpha/r$, where K is a constant and α the angle which the radius vector r makes with the slip direction. The probability of finding carbon atoms in the upper half of the plane will no doubt be extremely small as the lattice in this region is in a state of compression. Since the elastic theory breaks down very near the centre of the dislocation, the above formula does so also. Nevertheless, it gives some valuable information regarding the probable distribution of carbon atoms. Since the probability that a carbon atom goes very near the centre of the dislocation in the region A (Figure 1) is greatest, it is reasonable to assume that this position will always be occupied by a carbon atom in every atomic plane. Now Cottrell and Bilby's calculations show that only about two carbon atoms can go within an annular region bounded by circles of radii 2 A. and 20 A. of each atomic plane; and since in any atomic plane there are several equivalent positions for the second carbon

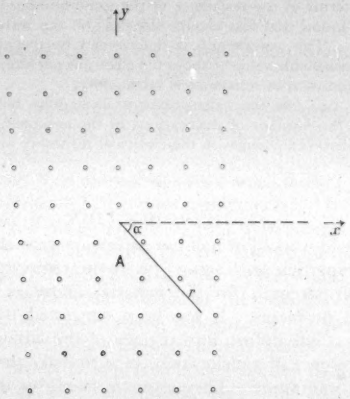

Figure 1.

atom, one may assume that the positions of the second carbon atom in different planes are random. This means that during the aging process, near the edge of each dislocation, a single row of carbon atoms parallel to the edge is formed. There will naturally be some deviations in the positions of the carbon atoms from the straight row. The root mean square of these deviations from the straight line, however, will be small in comparison with the wavelength of the electrons, whose scattering is responsible for the electrical resistance, and hence to a first approximation these deviations may be neglected in calculating the probability for scattering of these electrons (see § 3(*a*)).

Since a carbon atom occupying an interstitial position in the unstrained iron lattice has a tendency to expand the lattice locally, migration of carbon atoms into the dilated parts of the lattice due to a dislocation makes the strain and hence the dislocation more stable by relieving the stress, but does not appreciably affect the magnitude of the strain. Hence any change in the electrical properties of the specimen with aging must be due to the rearrangement of carbon atoms in the form of rows alone.

§ 3. THE CALCULATION OF ELECTRICAL RESISTANCE

The calculation of electrical resistance of a metal or an alloy consists of three steps: (*a*) the calculation of the probability that an electron makes a transition from a state $\mathbf{k}$ to an element dS' of the surface in $\mathbf{k}$-space having the same energy—this is denoted by $P(\mathbf{kk}')dS'$; (*b*) the calculation of relaxation time; (*c*) the calculation of electrical conductivity.

(*a*) *Calculation of the Probability* $P(\mathbf{kk}')dS'$

This probability per unit time per unit volume is given by

$$P(\mathbf{kk}')\,dS' = \frac{1}{4\pi^2\hbar}\cdot\frac{dS'}{dE/dk_n}\left|\int\psi_{\mathbf{k}}^{*}U\psi_{\mathbf{k}'}\,d\tau\right|^2, \qquad \ldots\ldots(1)$$

(see Mott and Jones 1936, p. 251, formulae (14) and (15)), in which $\psi_{\mathbf{k}}$ and $\psi_{\mathbf{k}'}$ are the wave functions of the incident and the scattered electrons respectively and U is the deviation of the potential from the periodic potential of the ideal lattice. The integration is over the whole volume of the material.

When a metal contains only a few foreign atoms—as in our problem—the contribution to U comes only from these foreign atoms; this may be taken to be finite only in the sphere whose volume is of the order of the atomic volume. Hence denoting by U_n the potential round the nth foreign atom, the perturbing potential U can be written as

$$U=\sum_n U_n \qquad \ldots\ldots(2)$$

where the summation is over all the foreign atoms. When the foreign atoms are distributed at random in the lattice, the value of the integral in (1) is usually evaluated at each foreign atom and the total probability of scattering due to all the foreign atoms obtained by multiplying by the number of foreign atoms. This actually amounts to adding up the intensities of the electron waves scattered from different atoms. However, in our problem the carbon atoms in the dislocations are not distributed at random in the iron lattice and hence we have to add up the amplitudes of the electron waves scattered from these carbon atoms. For this purpose the integral in (1) may be written as

$$\int\psi_{\mathbf{k}}^{*}U\psi_{\mathbf{k}'}\,d\tau=\int\psi_{\mathbf{k}}^{*}\sum_n U_n\psi_{\mathbf{k}'}\,d\tau. \qquad \ldots\ldots(3)$$

Now by a theorem of Bloch, $\psi_{\mathbf{k}}$ and $\psi_{\mathbf{k}'}$ are of the form $e^{i\mathbf{k}.\mathbf{r}}u_{\mathbf{k}}(x,y,z)$ and $e^{i\mathbf{k}'.\mathbf{r}}u_{\mathbf{k}'}(x,y,z)$ where $u_{\mathbf{k}}(x,y,z)$ and $u_{\mathbf{k}'}(x,y,z)$ are periodic with the period of the lattice and may be taken to be spherically symmetrical for a cubic metal.* We can, therefore, replace the integral over the whole volume by a summation over all the carbon atoms and integration over a single atomic sphere. Doing so, we have

$$\int e^{i(\mathbf{k}-\mathbf{k}').\mathbf{r}}u_{\mathbf{k}'}^{*}(\sum_n U_n)u_{\mathbf{k}}\,d\tau=\sum_n e^{i(\mathbf{k}-\mathbf{k}').\mathbf{r}_n}\int u_{\mathbf{k}}^{*}U_n u_{\mathbf{k}}e^{i(\mathbf{k}-\mathbf{k}').(\mathbf{r}-\mathbf{r}_n)}\,d\tau'$$

where $d\tau'$ refers to integration over the atomic sphere round the nth carbon atom. The integral obviously is independent of the particular carbon atom chosen and may be taken before the summation sign. Hence (1) may be written as

$$P(\mathbf{kk}')dS'=f_0^2dS'\left|\sum_n e^{i(\mathbf{k}-\mathbf{k}').\mathbf{r}_n}\right|^2, \qquad \ldots\ldots(4)$$

* The magnitude of the wave-vector $\mathbf{k}$ in iron may be determined by applying the free electron formula to the electrons in the 4s band. The holes in the 3d band are assumed not to contribute appreciably to the conductivity since their effective mass is very large in comparison with those of 4s electrons.

where f_θ^2 may be termed the "scattering power" of a single carbon atom dissolved in the iron lattice as a function of θ, and the summation in (4) is over all carbon atoms. f_θ^2 is defined by

$$f_\theta^2 = \frac{1}{4\pi^2\hbar}\left(\frac{dE}{d\mathbf{k}_n}\right)^{-1}\left|\int u_{\mathbf{k}'}^* U_n u_{\mathbf{k}} e^{i(\mathbf{k}-\mathbf{k}').(\mathbf{r}-\mathbf{r}_n)}\, d\tau.\right|^2.$$

We shall assume in what follows that f_θ^2 does not change appreciably due to strains in the iron lattice.

We now apply formula (4) to calculate $P(\mathbf{kk}')$ for rows of carbon atoms. Let the distance between two neighbouring carbon atoms in a row along the z axis be a. Then if there are n atoms in the row, $P(\mathbf{kk}')$ due to such a row of atoms will be given by

$$P_1(\mathbf{kk}') = f_\theta^2\left|\sum_{n=0}^{n-1}\exp\{i(\mathbf{k}-\mathbf{k}')_z na\}\right|^2$$

$$= f_\theta^2 \sin^2\{\tfrac{1}{2}na(\mathbf{k}-\mathbf{k}')_z\}/\sin^2\{\tfrac{1}{2}a(\mathbf{k}-\mathbf{k}')_z\}, \qquad \ldots\ldots(5)$$

where $(\mathbf{k}-\mathbf{k}')_z$ is the z component of the vector $\mathbf{k}-\mathbf{k}'$. If there are N dislocations *in all* in the alloy, with their edges parallel to the z axis and their centres distributed randomly in the x–y plane, then $P_1(\mathbf{kk}')$ due to N rows of carbon atoms will be given by

$$P_1(\mathbf{kk}') = Nf_\theta^2 \sin^2\{\tfrac{1}{2}na(\mathbf{k}-\mathbf{k}')_z\}/\sin^2\{\tfrac{1}{2}a(\mathbf{k}-\mathbf{k}')_z\}. \qquad \ldots\ldots(6)$$

In addition the electrons will be scattered by thermal motions, internal strains and by any remaining carbon atoms which are distributed randomly throughout the crystal. If the number of such carbon atoms be n_2, then the probability of scattering due to them will be given by

$$P_2(\mathbf{kk}') = n_2 f_\theta^2. \qquad \ldots\ldots(7)$$

Denoting the probability of scattering due to thermal motions and internal strains by $P_3(\mathbf{kk}')$, the total probability $P(\mathbf{kk}')$ is given by

$$P(\mathbf{kk}') = P_1(\mathbf{kk}') + P_2(\mathbf{kk}') + P_3(\mathbf{kk}'). \qquad \ldots\ldots(8)$$

(*b*) *Calculation of Relaxation Time*

The relaxation time for the electrons is given by the well known integral equation

$$-1 = \int P(\mathbf{kk}')\{(\mathbf{k}'_F/\mathbf{k}_F)\tau_{\mathbf{k}'} - \tau_{\mathbf{k}}\}\, dS', \qquad \ldots\ldots(9)$$

where the integration over dS' refers to integration over all portions of the Fermi surface, $\tau_{\mathbf{k}}$ and $\tau_{\mathbf{k}'}$ are the relaxation times in directions $\mathbf{k}$ and $\mathbf{k}'$, and $\mathbf{k}'_F$ and $\mathbf{k}_F$ denote the components of $\mathbf{k}'$ and $\mathbf{k}$ respectively along the direction of the applied electric field F. Assuming the Fermi surface in $\mathbf{k}$-space to be spherical in the absence of the electric field, we may to a first approximation write in (9) $dS' = k^2 dw'$, where dw' is an element of solid angle and k is the radius of the Fermi sphere.*

Let F make an angle μ with the z axis and let the plane containing the z axis and F be the z–x plane. Remembering that both $P_2(\mathbf{kk}')$ and $P_3(\mathbf{kk}')$ are functions of the angle of scattering alone, it is obvious from the form of $P_1(\mathbf{kk}')$ that the assumption in the previous sentence does not involve any loss of generality.

* In addition to the s–s transitions considered above, there will be scattering of electrons due to s–d transitions. Since neither the mechanism of the s–d transitions nor their contribution to electrical resistance is clear (Seitz 1940), we shall neglect the effect of these transitions on scattering of electrons by carbon atoms.

Further let **k** make an angle β with the z axis and let the plane containing **k** and the z axis make an angle ψ with the plane containing the z and x axes and let α and ϕ denote the corresponding angles for **k′**. Then the integral equation (9) can be written as

$$\tau_{\mathbf{k}} k^2 \int P(\mathbf{kk'}) d\omega' = 1 + k^2 \int P(\mathbf{kk'}) \tau_{\mathbf{k'}} \left(\frac{\sin\mu \sin\alpha \cos\phi + \cos\mu \cos\alpha}{\sin\mu \sin\beta \cos\psi + \cos\mu \cos\beta} \right) d\omega'. \quad \ldots\ldots(10)$$

In terms of these angles

$$d\omega' = \sin\alpha \, d\alpha \, d\phi; \qquad \cos\theta = \sin\alpha \sin\beta \cos(\phi - \psi) + \cos\alpha \cos\beta \quad \ldots\ldots(11)$$

and

$$P_1(\mathbf{kk'}) = N f_\theta^2 \sin^2\{\tfrac{1}{2} nka(\cos\beta - \cos\alpha)\} / \sin^2\{\tfrac{1}{2} \kappa a(\cos\beta - \cos\alpha)\}. \quad \ldots\ldots(12)$$

In order to solve (10) we must know the variations of f_θ^2 and $P_3(\mathbf{kk'})$ with the angle of scattering θ. Since this is difficult to obtain we shall assume that both are isotropic, i.e. independent of the directions of **k** and **k′** separately and of the angle θ between them. As the potential round any carbon atom may be regarded as spherical, and as the contribution to $P_3(\mathbf{kk'})$ due to strains is small, the first assumption is justified. Further, since the number of electrons in the 4s band of iron is small ($\sim$0·6 per atom, see § 4) the wavelength of the Fermi electrons is sufficiently large to justify the second assumption to a first approximation. Then if we write

$$k^2 \int f_\theta^2 \, d\omega' = \eta \quad \ldots\ldots(13)$$

and

$$k^2 \int P_3(\mathbf{kk'}) \, d\omega' = \chi_3, \quad \ldots\ldots(14)$$

we have

$$\chi_2 = k^2 \int P_2(\mathbf{kk'}) \, d\omega' = n_2 \eta \quad \ldots\ldots(15)$$

and

$$\chi_1 = k^2 \int P_1(\mathbf{kk'}) \, d\omega' = \tfrac{1}{2} N\eta \int_0^\pi \frac{\sin^2\{\tfrac{1}{2} nka(\cos\beta - \cos\alpha)\}}{\sin^2\{\tfrac{1}{2} ka(\cos\beta - \cos\alpha)\}} \sin\alpha \, d\alpha. \quad \ldots\ldots(16)$$

The integrand in (16) has a very strong maximum at $\alpha = \pm\beta$ and the limits of integration are such that the second maximum at

$$\tfrac{1}{2} ka(\cos\beta - \cos\alpha) = \pi \quad \ldots\ldots(17)$$

is not reached since the wavelength is larger than twice the interatomic distance. Hence (16) reduces to

$$\chi_1 = k^2 \int P_1(\mathbf{kk'}) \, d\omega' = Nn\eta(\pi/ka) = n_1 \eta(\pi/ka), \quad \ldots\ldots(18)$$

where n_1 denotes the total number of carbon atoms in all the dislocations. It is seen that none of these integrated values depend on the incident direction **k**. An occasional gap in a row of carbon atoms will not affect the results, since so long as the length of the rows is large compared with the wavelength, formula (18) holds and χ_1 depends only on the total number of carbon atoms that have gone into the rows.

The integral equation (10) can now be written

$$\tau_{\mathbf{k}} = \frac{1}{\chi} + \frac{k^2}{\chi} \int \{P_1(\mathbf{kk'}) + P_2(\mathbf{kk'}) + P_3(\mathbf{kk'})\} \tau_{\mathbf{k'}} \left\{ \frac{\sin\mu \sin\alpha \cos\phi + \cos\mu \cos\alpha}{\sin\mu \sin\beta \cos\psi + \cos\mu \cos\beta} \right\} d\omega', \quad \ldots\ldots(19)$$

where $\chi = \chi_1 + \chi_2 + \chi_3$.

This is the Fredholms integral equation of the second kind and its solution can be obtained by the Liouville–Neumann method in the form of an infinite series (Margenau and Murphy 1943). The evaluation of different terms in the series becomes particularly simple in view of the assumed isotropy of $P_2(\mathbf{kk}')$ and $P_3(\mathbf{kk}')$. The infinite series obtained as a solution of (19) is convergent and can be summed giving

$$\tau_{\mathbf{k}} = \frac{1}{\chi}\left[1+\frac{\chi_1}{\chi}\frac{\cos\mu\cos\beta}{\sin\mu\sin\beta\cos\psi+\cos\mu\cos\beta}\left\{1+\left(\frac{\chi_1}{\chi}\right)+\left(\frac{\chi_1}{\chi}\right)^2+\ldots.\right\}\right]$$

$$= \frac{1}{\chi}\left[1+\frac{\chi_1}{\chi-\chi_1}\frac{\cos\mu\cos\beta}{\sin\mu\sin\beta\cos\psi+\cos\mu\cos\beta}\right] \qquad \ldots\ldots(20)$$

since $\chi_1 < \chi$. The solution may be verified by substitution in equation (19).

(c) *Calculation of Electrical Conductivity*

The specific conductivity is given by (Mott and Jones 1936, p. 262, equation (52)).

$$\sigma = -\frac{2e^2}{\hbar^2}\frac{1}{(2\pi)^3}\iiint \tau_{\mathbf{k}}\frac{dE}{d\mathbf{k}}\left(\frac{k_F}{k}\right)^2\frac{df_0}{dk}\,dk_x dk_y dk_z. \qquad \ldots\ldots(21)$$

Taking the spherical polar coordinates for $\mathbf{k}$, as before, (21) becomes

$$\sigma = -\frac{2e^2}{\hbar^2}\frac{1}{(2\pi)^3}\iiint \tau_{\mathbf{k}}\frac{dE}{dk}(\sin\mu\sin\beta\cos\psi+\cos\mu\cos\beta)^2\frac{df_0}{dk}k^2\sin\beta\,d\beta\,d\psi\,dk.$$

Since (df_0/dk) is finite only in a very small range of k at the surface of the Fermi distribution, while integrating with respect to k we keep all other terms as constant at $k=k_{\max}$ and, with $\int(df_0/dk)\,dk=-1$, we have

$$\sigma = \frac{e^2}{4\pi^3\hbar^2}\left(k^2\frac{dE}{dk}\right)_{k=k_{\max}}\iint\tau_{\mathbf{k}}(\sin\mu\sin\beta\cos\psi+\cos\mu\cos\beta)^2\sin\beta\,d\beta\,d\psi$$

$$= N_{\text{eff}}\frac{e^2}{m}\frac{3}{4\pi}\int_{\beta=0}^{\pi}\int_{\psi=0}^{2\pi}\tau_{\mathbf{k}}(\sin\mu\sin\beta\cos\psi+\cos\mu\cos\beta)^2\sin\beta\,d\beta\,d\psi, \qquad \ldots\ldots(22)$$

where N_{eff} is the effective number of free electrons per unit volume * and is given by

$$N_{\text{eff}} = \left\{\frac{8\pi}{3}\left(\frac{k}{2\pi}\right)^3\frac{m}{\hbar^2 k}\frac{dE}{dk}\right\}_{k=k_{\max}}; \qquad \ldots\ldots(23)$$

(Mott and Jones 1936, Chap. III, §4).

Now substituting for $\tau_{\mathbf{k}}$ from equation (20) and integrating, we have

$$\sigma = N_{\text{eff}}\frac{e^2}{m}\cdot\frac{1}{\chi}\left[1+\frac{\chi_1}{\chi-\chi_1}\cos^2\mu\right]. \qquad \ldots\ldots(24)$$

It is obvious from (24) that when $\mu=0$, that is when the direction of applied electric field is along the z axis, the conductivity is a maximum and equal to $N_{\text{eff}}e^2/m(\chi_2+\chi_3)$. This means that the rows of carbon atoms do not offer any resistance to an electric current flowing along their direction. This can be seen from general considerations also, as follows. It is clear from expression (12) for $P_1(\mathbf{kk}')$ that, for a given direction $\mathbf{k}$ of the incident electrons, $P_1(\mathbf{kk}')$ is finite

* N_{eff} will be equal to the number of electrons in the 4s band of iron.

only in the neighbourhood of those directions of $\mathbf{k}'$ for which the z component of the momentum remains unaltered. Hence if the electric field is applied along the z direction the scattering by the rows of carbon atoms will not obstruct the flow of the current in this direction.

It can also be seen from (24) that the conductivity is least for $\mu=\frac{1}{2}\pi$, when $\sigma=N_{\text{eff}}e^2/m\chi$ or the specific resistance

$$R=(m/N_{\text{eff}}e^2)\chi=(m/N_{\text{eff}}e^2)(\chi_1+\chi_2+\chi_3)$$

is a maximum. If all the carbon atoms present in iron go into rows then for $\mu=\frac{1}{2}\pi$,

$$R=(m/N_{\text{eff}}e^2)(\chi_1+\chi_3),$$

as compared with $R=(m/N_{\text{eff}}e^2)(\chi_2+\chi_3)$ when the carbon atoms are distributed at random. Now for the same number of carbon atoms

$$(\chi_1/\chi_2)=c=(\pi/ka) \qquad \ldots\ldots(25)$$

and since $N_{\text{eff}}\sim 0{\cdot}5$ per atom (see § 4) and k can be obtained from the formula

$$8\pi k^3/3=(2\pi)^3N_{\text{eff}}, \qquad \ldots\ldots(26)$$

we have $c\sim 1{\cdot}3$. This would correspond to an increase in the resistance for current in this direction.

On the other hand if one is experimenting with a polycrystal or a very much hardened crystal, so that the rows of carbon atoms can have all possible orientations with the direction of the applied electric field, then the observed electrical resistance will be the average given by

$$R_{\text{av}}=\frac{m}{N_{\text{eff}}e^2}\frac{\int_0^{\pi}\int_0^{2\pi}\left[\dfrac{\chi(\chi-\chi_1)}{\chi-\chi_1+\chi_1\cos^2\mu}\right]\sin\mu\,d\mu\,d\epsilon}{\int_0^{\pi}\int_0^{2\pi}\sin\mu\,d\mu\,d\epsilon}=\frac{m\chi}{N_{\text{eff}}e^2}\left\{\left(\frac{\chi}{\chi_1}-1\right)^{\frac{1}{2}}\tan^{-1}\left(\frac{\chi}{\chi_1}-1\right)^{-\frac{1}{2}}\right\}. \qquad \ldots\ldots(27)$$

§ 4. COMPARISON WITH EXPERIMENTAL DATA

In a cold worked material, there are about 10^{11} or 10^{12} dislocation lines per unit area (Seitz 1943). Since, as we have seen, one can assume that on aging only one row of carbon atoms is formed in each dislocation, the number of carbon atoms taking part in the formation of rows will be given by the following table:

No. of dislocation lines per unit area ..	10^{11}	10^{12}
No. of carbon atoms per unit volume ..	$3{\cdot}8\times10^{18}$	$3{\cdot}8\times10^{19}$
No. of carbon atoms in atomic per cent ..	$0{\cdot}46\times10^{-2}$	$4{\cdot}6\times10^{-2}$
No. of carbon atoms in weight per cent ..	0·001	~0·01

The number of atoms per cm^3 in iron are $8{\cdot}55\times10^{22}$.

Now 0·01 weight percent carbon increases the electrical resistance of iron at room temperature by 2·5% (Dijkstra 1947). Hence, using the fact that $\chi_1/(\chi-\chi_1)\ll 1$, we have from equations (24) and (27),

$$R=(m/N_{\text{eff}}e^2)(\chi_3+\chi_2+\chi_1\sin^2\mu) \qquad \ldots\ldots(28)$$

$$=R_2+R_1\sin^2\mu, \text{ say} \qquad \ldots\ldots(29)$$

and

$$R_{\text{av}}=R_2+2R_1/3 \qquad \ldots\ldots(30)$$

where R_2 is the specific resistance due to thermal vibrations, internal strains and due to any carbon atoms distributed at random, and $R_1 \sin^2\mu$ is the resistance due to rows of carbon atoms. If R_0 is the specific resistance of the specimen before aging, i.e. when *all* the carbon atoms in the specimen are distributed at random, we have from (25)

$$R_0 = R_2 + R_1/c. \qquad \ldots\ldots(31)$$

In Figure 2, R_0 and R are plotted in arbitrary units against μ. Curves (*a*) and (*b*) represent the values of R when $N_{\text{eff}} \sim 1$ per atom ($c \sim 1{\cdot}1$) and when $N_{\text{eff}} \sim 0{\cdot}6$ per atom ($c \sim 1{\cdot}3$). The origin refers to the value R_2.

For the case in which the directional distribution of the rows of carbon atoms is random, we can express the diminution in resistance in the form

$$R_d = \Delta R(1 - 2c/3) \qquad \ldots\ldots(32)$$

where c is given by (25) and ΔR is the resistance due to the *same* number of carbon atoms distributed at random as go into the rows on aging.

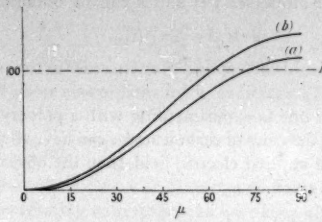

Figure 2.

In order to be able to compare the value of R_d as obtained from (32) with experimental values, we have to know c. It is by no means easy to decide a value of N_{eff} for iron. Manning (1943) has made some calculations for the number of electrons in the 4s band of iron, or N_{eff}, as 0·26 per atom. This value, however, seems to be too low, since the binding energy and electrical conductivity of iron are of the same order of magnitude as those of nickel and cobalt, for which the number of free electrons is ~0·6 per atom (Mott 1935). From the data on saturation magnetic moments of alloys of iron with Mn, Cr, Co and Ni, Slater (1936) also was led to assume the *same* value of 0·6 per atom for N_{eff} for *all* the three elements Ni, Co and Fe. We shall, therefore, assume that N_{eff} for iron is 0·6 electrons per atom. Using (26) we have $c \sim 1{\cdot}3$ and $R_d = 0{\cdot}4\Delta R/3$ as compared with $c \sim 1{\cdot}1$ and $R_d = 0{\cdot}7\Delta R/3$ if $N_{\text{eff}} \sim 1$ per atom.

Assuming that there are 10^{12} dislocation lines per cm², then since $\Delta R = 2{\cdot}5\%$ of the resistance of pure iron, $R_d = 0{\cdot}3\%$ of the resistance of pure iron, as compared with the observed value of about 0·2%. This should be regarded as a fair agreement with theory, in view of the various simplifying assumptions involved in the theory and an arbitrary assumption about the number of dislocations.

It may be pointed out that if one uses a single crystal which is worked in such a way that all the dislocation lines are parallel to each other, one can determine both c and the number of carbon atoms gone into the dislocations to form rows, and hence the number N of dislocations themselves, from (29) and the *observed variation* of the specific resistance with the directions of the applied field. It is

hoped that experiments of this type on single crystals when carried out will give some valuable information regarding the number of dislocations at various stages of hardening.

§ 5. THERMOELECTRIC POWER

It is clear from expressions (15) and (18) that the electrical resistance of carbon atoms depends on the wave number k (or the energy E) of the electrons at the Fermi surface in a different manner, according as the atoms are arranged in rows or are distributed at random. Hence, since the thermoelectric power is proportional to $d(\log R)/dE$, it is obvious that on *aging* the specimen will show a change in the thermoelectric power. This change naturally will vary with the direction of the applied electric field when all the dislocation lines are parallel in the crystal, and hence can be utilized to determine c and N, provided one knows the dependence on R (or E) of the resistance of pure iron and that of the carbon atoms distributed at random in it. The required dependence can be easily obtained from the measurements of Dupuy and Portevin (1912) on the thermoelectric power of iron of low carbon content.

For a polycrystal also c and N can be determined by comparing the observed changes in both the specific resistance and the thermoelectric power with suitable equations from the theory.

ACKNOWLEDGMENTS

The author wishes to thank Professor N. F. Mott for suggesting the problem and for his continued interest in the work, and Dr. J. K. Galt for many helpful discussions. Thanks are also due to the Commissioners of the 1851 Exhibition for financial support.

REFERENCES

Cottrell, A. H., and Bilby, B. A., 1949, *Proc. Phys. Soc.* A, **62,** 49.

Dijkstra, L. J., 1947, *Philips Res. Rep.*, p. 357.

Dupuy, E. L., and Portevin, A., 1912, *C. R. Acad. Sci., Paris,* **135,** 1,082.

Manning, M. F., 1934, *Phys. Rev.*, **63,** 190.

Margenau, H., and Murphy, G. M., 1943, *Mathematics of Physics and Chemistry* (New York : D. Van Nostrand Co. Inc.), p. 504.

Mott, N. F., 1935, *Proc. Phys. Soc.*, **47,** 571.

Mott, N. F., and Jones, H., 1936, *The Theory of Properties of Metals and Alloys* (Oxford : University Press).

Seitz, F., 1940, *Theory of Solids* (London and New York : McGraw-Hill Book Co.), p. 535; 1943, *The Physics of Metals* (London and New York : McGraw-Hill Book Co.), p. 94.

Slater, J. C., 1936, *Phys. Rev.*, **49,** 931.

A Calculation of the Solubility Limits of the Copper–Silver System

By M. K. I. ARAFA

Mathematics Department, Imperial College, London S.W.7

Communicated by H. Jones; *MS. received* 26*th June* 1948

ABSTRACT. A calculation is made of the change in the energy of a monovalent metal when one of its atoms is replaced by an atom of a different monovalent metal, not necessarily of the same atomic volume. From a knowledge of this energy the heat of solution can be determined and thereby, through the usual thermodynamic relations, also the solubility limits. Numerical calculations have been carried out for the copper–silver system and the theory shows in this case the existence of narrow solubility limits, in agreement with the known phase diagram. The theoretical values of the heats of solution are compared with those required to give the observed solubility limits.

§ 1. INTRODUCTION

In this paper, an attempt is made to calculate the heat of solution when one monovalent metal is dissolved in another and thus to find, through the usual thermodynamic relations, the position of the solubility limits where such limits exist.

In the case when the constituent metals have different valencies it has been shown that the Fermi energy, determined by the Brillouin zone structure, is mainly responsible for the solubility limits and this led to a qualitative explanation of the Hume-Rothery rules (Jones 1934). However, for the case in which the solute and solvent metals have the same valency, very little work on the calculation of the energy of an alloy as a function of its composition has hitherto been carried out.

The copper–silver system was chosen for detailed calculations because, in the first place, solubility limits are known to exist, and secondly because Hartree self-consistent fields of the copper and silver ions, which are required in the calculations, are available.

The following treatment is based on the general ideas of the Wigner and Seitz theory of the constitution of pure metals. The main difference arises from the fact that the potential in the alloy is no longer periodic and this requires a somewhat different method of calculating the Fermi energy.

In § 2 the heat of solution is defined and a relation between the temperature and the atomic concentration is obtained. In § 3 a method for obtaining one-electron wave functions in an alloy is described. The change in the Fermi energy of a metal when a foreign atom replaces one of its atoms is dealt with in § 4 and § 5. The change in the total energy is considered in § 6.

§ 2. THE HEAT OF SOLUTION

The energies of all the metals considered are defined with reference to the same zero level of energy, which is taken to be the energy of all the ions and electrons at infinite separation.

Consider an alloy of two metals A and B. Let c_1 and c_2 be the atomic concentration of B in two phases of the alloy, and f_1 and f_2 be the free energies per atom of

these phases respectively. The conditions for the equilibrium of these phases, at a common temperature T, are $\partial f_1/\partial c_1 = \partial f_2/\partial c_2 = (f_1 - f_2)/(c_1 - c_2)$. If c_v denotes the heat capacity per atom at constant volume, and $E(c)$ the energy per atom at the absolute zero, the free energy per atom of a phase at concentration c and temperature T may be assumed to be given by the following equation :

$$f(c, T) = kT\{c \ln c + (1-c)\ln(1-c)\} + E(c) + \int_0^T c_v dT - T\int_0^T c_v dT/T.$$

Applying the previous equilibrium conditions and assuming that the change in c_v is negligible when c varies, it can be deduced for dilute solutions that the concentration c of metal B is given approximately by

$$kT \ln c = E(1) - E(0) - [\partial E(c)/\partial c]_{c=0} \qquad \ldots\ldots(1)$$

where $E(1)$ and $E(0)$ are the energies per atom of the pure metals B and A respectively.

If N_B denotes the number of atoms of type B and N the total number in a given lattice, then $\partial E/\partial c = [\partial(NE)/\partial N_B]_N$ and, therefore, $[\partial E/\partial c]_{c\to 0}$ denotes the change in the energy of the lattice, of a dilute solid solution of N atoms, where one atom of A is replaced by one atom of B. Hence $W = E(1) - E(0) - [\partial E/\partial c]_{c=0}$ is the energy liberated when an atom of metal B is taken from the pure metal B and put into the dilute solid solution of B in A. The quantity so defined is called the heat of solution. Phase boundaries exist when W is negative, that is to say when work must be performed to add a solute atom to the solid solution. The quantity $E(1) - E(0)$ is known, since for either metal $E = -(S + I)$ where S is the heat of sublimation (Grimm and Wolff 1934) and I is the ionization potential of the atom; hence we can determine the solubility limits if we can calculate $[\partial E/\partial c]_0$.

§ 3. THE VALENCE ELECTRON WAVE FUNCTIONS

Consider a lattice of copper atoms in which a single copper atom is replaced by a silver atom. Both copper and silver have a face-centred cubic structure and it will be assumed that the interatomic distance d of the twelve nearest neighbours of an atom is not changed by the presence of the foreign atom. If at a point at a distance x from the silver atom, along each line of the nearest neighbours, a plane is drawn perpendicular to that line, then these twelve planes will enclose a dodecahedron around the silver atom. Let the position vector of the silver atom be $\mathbf{r}_0$ and that of a copper atom be $\mathbf{r}_n$. Inside this dodecahedron the potential energy of an electron is taken to be $V_{Ag}(\mathbf{r} - \mathbf{r}_0) + C(r)$ and outside it, in the neighbourhood of the copper ion at $\mathbf{r}_n$, which is nearest to $\mathbf{r}$, the potential energy is taken to be $V_{Cu}(\mathbf{r} - \mathbf{r}_n)$. V_{Ag} and V_{Cu} are the potential energies of an electron in the fields of a single silver ion and a single copper ion respectively, defined so that they vanish as $1/r$ at large distances, and $C(r)$ depends on the distribution of the electronic charge round the silver ion. If $C(r)$ is known, then for a given choice of the distance x the potential energy of an electron anywhere in the lattice is determined, and may be denoted by $V(\mathbf{r})$.

If the one-electron wave functions could be found in the field of this potential, then the total wave function could be written as a product of two determinants, and the expectation value of the exact Hamiltonian operator calculated. The Hamiltonian operator H is given by :

$$H = \sum_{i=1}^{N} H_0(\mathbf{r}_i) + \sum\sum_{i>j} \frac{2}{r_{ij}} + \sum\sum_{a>b} \frac{2}{r_{ab}}, \qquad \ldots\ldots(2)$$

where $H_0(\mathbf{r}_i) = -\nabla_i^2 + \sum_a V_a(\mathbf{r}_i)$, $\mathbf{r}_i$ is the position vector of the ith electron, r_{ij} the distance between the ith and jth electrons, r_{ab} the distance between the ions a and b and N is the total number of electrons in the lattice. In this expression the unit of energy is taken to be the Rydberg unit, viz. 13·53 ev., and the unit of length the radius of the first Bohr orbit.

The best values to take for x and $C(r)$ would be, according to the variation principle. those which minimize the total energy calculated in this way. As a zero approximation $C(r)$ has been assumed to be equal to zero, and the distance x to be fixed by the condition

$$V_{Ag}(x) = V_{Cu}(d-x). \qquad \ldots\ldots(3)$$

It will be shown that there is either an accumulation or a diminution of charge round a foreign atom and thus a value of $C(r)$ which is different from zero would lower the total energy relative to the zero approximation. If q_e denotes the excess charge at the foreign atom, then C will be of the order of magnitude q_e/r_0 where r_0 is the radius of the atomic sphere. In some cases, this will be far from negligible, and it would then be necessary to proceed to higher approximations.

The one-electron wave functions ψ with energy E, have been obtained in the following way. Write $\psi(\mathbf{r}) = \chi(\mathbf{r}) \cdot u(\mathbf{r})$ and $E = \epsilon + \epsilon_0$, then the wave equation, expressed in Rydberg units of energy and lengths in units of the first Bohr orbit, can be written

$$u[\nabla^2\chi + \epsilon\chi] + \chi[\nabla^2 u + \{\epsilon_0 - V(\mathbf{r})\}u] = -2\nabla\chi \cdot \nabla u. \qquad \ldots\ldots(4)$$

For a pure metal $V(\mathbf{r})$ is periodic, and an approximate solution can be obtained, first by neglecting the term $2\nabla\chi \cdot \nabla u$, and secondly by equating both brackets on the left hand side to zero. This gives a solution of the form $\psi = u(\mathbf{r}) \cdot \exp(i\mathbf{k} \cdot \mathbf{r})$, where $k^2 = \epsilon$ is the energy of an electron relative to ϵ_0 which is the lowest eigenvalue corresponding to a solution in which u is periodic with the period of the lattice. With this approximation the total energy is given as that of the lowest state ϵ_0 plus a Fermi energy given by the free electron approximation.

An attempt is made now to determine the wave function of an electron in the copper lattice in which a silver atom replaces one copper atom. Defining a function $v(\mathbf{r})$ such that $v(\mathbf{r}) = \phi$ inside the polyhedron round the silver ion, where ϕ is a constant, and $v(\mathbf{r}) = 0$ outside this polyhedron, equation (4) can be written

$$u[\nabla^2\chi + \{\epsilon - v(\mathbf{r})\}\chi] + \chi[\nabla^2 u + \{\epsilon_0 + v(\mathbf{r}) - V(\mathbf{r})\}u] = -2\nabla\chi \cdot \nabla u. \qquad \ldots\ldots(5)$$

The Wigner and Seitz treatment of pure metals suggests that, as a first approximation, the term $2\nabla\chi \cdot \nabla u$ should be neglected and solutions of the following two equations sought :

$$\nabla^2 u + \{\epsilon_0 + v(\mathbf{r}) - V(\mathbf{r})\}u = 0 \qquad \ldots\ldots(6)$$

and

$$\nabla^2\chi + \{\epsilon - v(\mathbf{r})\}\chi = 0. \qquad \ldots\ldots(7)$$

Taking for the domain of the wave function a large sphere of radius L in which there is a single foreign atom at the centre, the boundary conditions are : (i) ψ vanishes over the sphere of radius L, (ii) ψ and ψ' are continuous everywhere inside this sphere.

To get the solutions of (6) outside the central polyhedron, that is where $v(\mathbf{r}) = 0$, each polyhedron round a copper ion is replaced by a sphere of the same volume and the boundary condition $u'(\mathbf{r}_0) = 0$ is applied over this sphere of radius r_0. This

approximation of replacing the polyhedron by a sphere leads to a small discontinuity in the derivative of $u(\mathbf{r})$ at the surfaces of the spheres, but Wigner and Seitz have shown that the error involved is negligible.

The solution of (6) inside the central polyhedron is obtained by replacing this polyhedron by a sphere of radius a which has the same volume, and using the conditions of continuity of u and u' at the surface of this sphere. It is clear from similarity that

$$a/x = r_0/\tfrac{1}{2}d = (2r_0 - a)/(d - x),$$

and since the potential of the ion at distances of order a or r_0 is practically the Coulomb potential it follows that

$$V_{Ag}(a)/V_{Cu}(2r_0 - a) = (2r_0 - a)/a = (d - x)/x = V_{Ag}(x)/V_{Cu}(d - x).$$

Thus condition (3) can be replaced by

$$V_{Ag}(a) = V_{Cu}(2r_0 - a). \qquad \ldots\ldots(8)$$

Taking the values of these potentials to be those given by the Hartree field (Hartree 1933, Black 1934–1935), (8) determines the radius of the central atomic sphere a. Within this sphere $V(\mathbf{r}) = V_{Ag}(\mathbf{r})$ and $v(\mathbf{r}) = \phi$ which is determined so as to assure

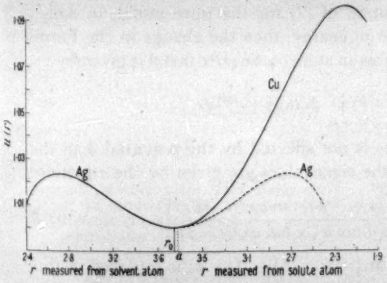

Figure 1. Full line represents the radial wave function in the alloy of Cu in Ag. Dotted line represents the radial wave function in the Ag pure metal.

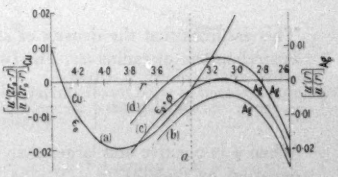

Figure 2. Illustrating the method of applying the boundary conditions for the determination of the wave function of the lowest state. Curve (*a*) $\epsilon_0 = -0{\cdot}75$. Curves (*b*), (*c*), (*d*) $\phi = 0{\cdot}05$, $0{\cdot}063$, $0{\cdot}08$, respectively.

the continuity of the wave function and its first derivative at the surface. Solving (6) for different values of ϕ a family of curves of $[u'(r)/u(r)]_{Ag}$ can be plotted and the solution which satisfies the condition

$$\left[\frac{u'(a)}{u(a)}\right]_{Ag} = -\left[\frac{u'(2r_0 - a)}{u(2r_0 - a)}\right]_{Cu} \qquad \ldots\ldots(9)$$

will be continuous to the same kind of approximation as the wave function obtained by Wigner and Seitz method for pure metals. Figure 1 shows the form of the wave functions obtained and Figure 2 shows how ϕ is obtained from the condition (9). It is found, in the case of a silver atom in a copper lattice, that $r_0 = 3{\cdot}3$, $a = 3{\cdot}34$ Bohr units and $\phi = 0{\cdot}063$ Rydberg units. In the case of a copper atom in a silver lattice $r_0 = 3{\cdot}75$, $a = 3{\cdot}72$ Bohr units and $\phi = -0{\cdot}046$ Rydberg units.

Equation (7) is the Schrödinger equation appropriate to the problem of a particle in a sphere of radius L in which the potential is zero everywhere except over a sphere of radius a, where it is constant and equal to ϕ. The solution can be written $\chi(r)=r^{-\frac{1}{2}}R(r)Y_{l,m}(\theta,\phi)$, where

$$R(r)=AJ_{l+\frac{1}{2}}(r\sqrt{(\epsilon-\phi)}), \qquad (0\leqslant r\leqslant a),$$

and

$$R(r)=BJ_{l+\frac{1}{2}}(r\sqrt{\epsilon})+CJ_{l-\frac{1}{2}}(r\sqrt{\epsilon}), \qquad (a\leqslant r\leqslant L).$$

$R(r)$ in the range $(0\leqslant r\leqslant a)$ is denoted by $R_1(r)$ and in the range $(a\leqslant r\leqslant L)$ by $R_2(r)$. The conditions $R_1(a)=R_2(a)$, $R_1'(a)=R_2'(a)$ and $R_2(L)=0$ determine the eigenvalue ϵ. Let $N_l(\epsilon)d\epsilon$ be the number of eigenvalues in the range from ϵ to $\epsilon+d\epsilon$ for given l, then the total energy of the electrons in the lattice relative to that of an electron in the lowest state will be

$$E_F=\sum_l(2l+1)\int_0^{\epsilon_F}N_l(\epsilon)\epsilon\,d\epsilon,$$

where ϵ_F is the maximum energy of an electron in the Fermi distribution relative to that of the lowest state. E_F is referred to as the Fermi energy.

§ 4. THE CHANGE IN THE FERMI ENERGY DUE TO THE PRESENCE OF A FOREIGN ATOM

If $\epsilon^{(0)}$ is the eigenvalue in the solution of (7) for the pure metal, in which $v(\mathbf{r})=0$, and $E_F^{(0)}$ the corresponding Fermi energy, then the change in the Fermi energy when a single foreign atom replaces an atom of the pure metal is given by :

$$E_F-E_F^{(0)}=\sum_l 2(2l+1)\int_0^{\epsilon_F}N_l(\epsilon)[\epsilon-\epsilon^{(0)}]\,d\epsilon.$$

This assumes that the density of states is not affected by the potential ϕ in the central sphere of radius a. For $l=0$ the eigenvalues are given by the equation,

$$\tan L\sqrt{\epsilon}=\left[\frac{\tan a\sqrt{\epsilon}-\sqrt{\{\epsilon/(\epsilon-\phi)\}}\tan a\sqrt{(\epsilon-\phi)}}{1+\sqrt{\{\epsilon/(\epsilon-\phi)\}}\tan a\sqrt{\epsilon}\tan a\sqrt{(\epsilon-\phi)}}\right]. \qquad \ldots\ldots(10)$$

When ϕ is positive and larger than ϵ, $\tan[a\sqrt{(\epsilon-\phi)}]/\sqrt{(\epsilon-\phi)}$ is replaced in this equation by $\tanh[a\sqrt{(\phi-\epsilon)}]/\sqrt{(\phi-\epsilon)}$. When $\phi=0$, i.e. in the case of a pure metal, the eigenvalues $\epsilon^{(0)}$ are the solutions of the equation $\tan(L\sqrt{\epsilon})=0$, which are

$$\epsilon^{(0)}=\pi^2n^2/L^2, \qquad n=1,2,3,\ldots. \qquad \ldots\ldots(11)$$

Since L is very large the left hand side of (10) fluctuates rapidly as ϵ increases whilst the right hand side is a slowly varying function of ϵ. Hence, without involving any essential approximation, ϵ can be replaced by $\epsilon^{(0)}$ in the right side of (10). If the right hand side of (10) is denoted by $\tan\zeta_0(\epsilon^{(0)})$, then

$$L\sqrt{\epsilon}=\zeta_0(\epsilon^{(0)})+n\pi, \qquad n=1,2,3,\ldots,$$

and using (11) the change in the eigenvalue of (7) may be written :

$$\epsilon-\epsilon^{(0)}=2L^{-1}\sqrt{\epsilon^{(0)}}\zeta_0(\epsilon^{(0)}). \qquad \ldots\ldots(11\,a)$$

Equations similar to (10) are also obtained for values of l different from zero; for $l=1$ the equation is

$$\tan L\sqrt{\epsilon}=\frac{-\phi/a\cot a\sqrt{\epsilon}+(\epsilon-\phi)\sqrt{\epsilon}+\epsilon\sqrt{(\epsilon-\phi)}\cot a\sqrt{\epsilon}\cot a\sqrt{(\epsilon-\phi)}}{\phi/a+(\epsilon-\phi)\sqrt{\epsilon}\cot a\sqrt{\epsilon}-\epsilon\sqrt{(\epsilon-\phi)}\cot a\sqrt{(\epsilon-\phi)}}. \qquad \ldots\ldots(12)$$

In each case let $\tan\zeta_l(\epsilon)$ denote the right hand side of these equations. Then $\tan L\sqrt{\epsilon}=\tan\zeta_l(\epsilon)$ and $L\sqrt{\epsilon}=\zeta_l(\epsilon^{(0)})+n\pi$, and the total change in the Fermi energy can be written

$$E_F-E_F^{(0)}=\Sigma_l 2(2l+1)\int_0^{\epsilon_F} N_l 2L^{-1}\sqrt{\epsilon}\zeta_l(\epsilon)\,d\epsilon. \qquad \ldots\ldots(13)$$

In this summation the contribution to $E_F-E_F^{(0)}$ of the terms corresponding to small values of l may be written

$$\Sigma_l 2(2l+1)\int_0^{\epsilon_F}\frac{1}{\pi}\zeta_l(\epsilon)\,d\epsilon, \qquad \ldots\ldots(14)$$

since for small values of l there is no appreciable difference between $N_l(\epsilon)$ and $N_0(\epsilon)$ which is equal to $L/2\pi\sqrt{\epsilon}$. By calculating numerically the sum (14), it is found that the terms corresponding to $l=0$, 1 and 2 are the most important, the others being negligible. Figure 3 shows the curves of the functions $\zeta_l(\epsilon)$ for these values

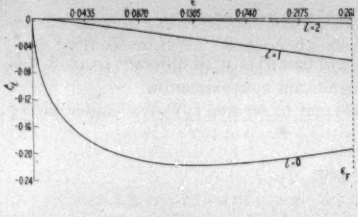

Figure 3. Displacement of the energy levels of the conduction electrons as given by equation (11*a*) due to a copper atom in solution in a silver lattice.

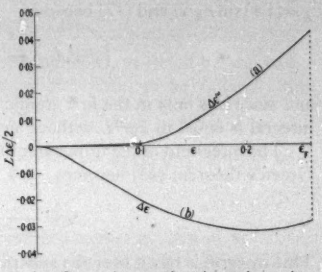

Figure 4. Correction to the eigenvalues given by (19). Curve (*a*) refers to the silver pure metal and (*b*) to the solution of copper in silver.

of l. For one silver atom dissolved in a copper lattice it is found that the change $E_F-E_F^{(0)}$ is 0·0588 Rydberg units, and when a copper atom replaces one of the atoms of a silver lattice the change is $-0{\cdot}0484$ Rydberg units.

§ 5. CORRECTIONS ARISING FROM THE TERM $2\nabla U.\nabla\chi$

In the previous section the eigenvalues of equation (4) have been obtained by neglecting the term $-2\nabla\chi.\nabla u$. The effect which this term has on the eigenvalues, and therefore on the total energy of the electrons, may be estimated by an application of the perturbation theory. If $\Delta\epsilon$ denotes the increase in the eigenvalue due to the term $-2\nabla\chi.\nabla u$ then, to the first order,

$$\Delta\epsilon=-\int\chi u.2\nabla\chi.\nabla u\,d\tau\Big/\int\chi^2u^2\,d\tau. \qquad \ldots\ldots(15)$$

This quantity will be shown to be of order $1/L$ and therefore makes no significant change to the energy of a pure metal. As Wigner and Seitz have shown, for the pure metal, it is necessary to consider the second order correction to the eigenvalues. Here, however, it is the change in the eigenvalues, brought about by the replacement of a solvent by a solute atom, which is of interest. This change is

itself of order $1/L$. Thus, in this case, even the first order term (15) will lead to a significant correction to the difference of the eigenvalues just mentioned.

In order to reduce the integrals of (15) first let

$$\overline{u^2(r)} = \frac{1}{4\pi r^2}\int_S u^2(r)\,dS, \qquad \ldots\ldots(16)$$

where the integration is over the surface of a sphere of radius r. This function of r must tend rapidly to a constant value, c^2, as r increases. In fact it may be assumed that $\overline{u^2}$ will only differ appreciably from c^2 within the central atomic sphere. The denominator of (15) may now be written

$$\int \chi^2 u^2\,d\tau = 4\pi\int_0^L r^2\chi^2\overline{u^2(r)}\,dr. \qquad \ldots\ldots(17)$$

It has been shown that the main contribution to the required energy change comes largely from those states for which $l=0$. The corrections required by the term $2\nabla\chi.\nabla u$ will, therefore, be calculated for these states only. For these states $\chi=(1/r)\sin r\sqrt{\epsilon}$, and (17) becomes

$$\int\chi^2u^2\,d\tau = 4\pi\int_0^L(\sin^2 r\sqrt{\epsilon})\overline{u^2(r)}\,dr,$$

and since it is only in the first atomic sphere that u^2 is at all different from c^2, this integral is equal to $2\pi c^2L$ without any significant approximation.

The integrand of the numerator of (15) may be written $(\chi\nabla\chi)\nabla u^2$ and applying Green's theorem (15) becomes

$$\Delta\epsilon = \frac{1}{2\pi c^2 L}\int u^2\nabla(\chi\nabla\chi)\,d\tau. \qquad \ldots\ldots(18)$$

This integral is taken over the sphere of radius L, and using (16), (18) reduces to

$$\Delta\epsilon = \frac{2}{L}\int_0^L\frac{\overline{u^2(r)}}{c^2}\frac{d}{dr}\left(r^2\chi\frac{d\chi}{dr}\right)dr.$$

Since $\int_0^L\frac{d}{dr}\left(r^2\chi\frac{d\chi}{dr}\right)dr=0$, (18) may be written :

$$\Delta\epsilon = \frac{2}{L}\int_0^L\left\{\frac{\overline{u^2(r)}}{c^2}-1\right\}\frac{d}{dr}\left(r^2\chi\frac{d\chi}{dr}\right)dr. \qquad \ldots\ldots(19)$$

The integrand of (19) becomes vanishingly small when r is appreciably greater than the radius of the central atomic sphere. It is assumed, therefore, that $\Delta\epsilon$ may be estimated by replacing the upper limit L by a in the integral of (19). When u and χ refer to the wave functions for the pure metal the energy correction is written $\Delta\epsilon^{(0)}$. When a solute atom occupies the central atomic sphere the appropriate functions u and χ, as calculated in § 3, are used in (19) to give $\Delta\epsilon$, and the correction to the energy difference is thus $\Delta\epsilon-\Delta\epsilon^{(0)}$. Figure 4 shows $\Delta\epsilon^{(0)}$ and $\Delta\epsilon$ calculated in this way for pure silver and for a silver lattice containing a copper atom respectively. The difference $\Delta\epsilon-\Delta\epsilon^{(0)}$ will be written $2\eta_0(\epsilon)/L$. In this calculation $\eta_0(\epsilon)$ has been determined only for the states $l=0$. For any other l the corresponding difference may be denoted by $\eta_l(\epsilon)$. The corrected change in the Fermi energy will be $(E_F-E_F^{(0)})+\Delta E_F$, where

$$\Delta E_F = \sum_l 2(2l+1)\int_0^{\epsilon_F}\frac{1}{\pi}\eta_l(\epsilon)\frac{d\epsilon}{\sqrt{\epsilon}}.$$

For a silver atom in a copper lattice the value of ΔE_F is 0·0063 Ryd., and for a copper atom in a silver lattice ΔE_F is $-0{\cdot}0133$ Ryd.

§ 6. THE CHANGE IN THE TOTAL ENERGY

As a zero approximation, it has been assumed in § 2, that the potential $C(r)$, due to the charge distribution round the foreign atom is zero. The calculated wave functions, based on this assumption, lead to a considerable change in the charge inside the central atomic sphere if the enclosed atom is replaced by a foreign one. In a silver lattice with one copper atom, the wave function outside the central atomic sphere is of the form

$$\psi_{l=0}(\mathbf{r}) = Ar^{-1}\sin\{(r-L)\sqrt{\epsilon}\}\,u_{Ag}(\mathbf{r}),$$

and inside this sphere

$$\psi_{l=0}(r) = Br^{-1}\sin\{r\sqrt{(\epsilon-\phi)}\}\,u_{Cu}(r).$$

From the continuity conditions it can be proved that

$$A^2/B^2 = [\epsilon+\phi\cos^2 a\sqrt{(\epsilon-\phi)}]/\epsilon,$$

and the value of the normalization factor A can be taken, as stated before, to be given by $1/A^2 = 2\pi c^2 L$. Taking the density of state $N(\epsilon)$ to be $L/2\pi\sqrt{\epsilon}$, the change in the central charge may be written as :

$$\frac{1}{\pi}\int_0^a \frac{u^2_{Cu}}{c^2}\,dr \int_0^{\epsilon_F} \frac{\sqrt{\epsilon}[1-\cos 2r\sqrt{(\epsilon-\phi)}]d\epsilon}{\phi[1+\cos 2a\sqrt{(\epsilon-\phi)}]+2\epsilon} - \frac{1}{\pi}\int_0^{r_s}[\sqrt{\epsilon_F}-\sin(2r\sqrt{\epsilon_F})/2r]\frac{u^2_{Ag}}{c^2}\,dr. \qquad \ldots\ldots(20)$$

(20) gives an accumulation of charge of 32% round a copper ion in a silver lattice, and a diminution of 29% in the charge round a silver ion in a copper lattice. This change in the charge distribution leads to a change in the potential energy of the lattice. If in a higher approximation $C(r)$ is taken to correspond to the altered charge given by (20), a different change in the charge distribution will be obtained. However, this second approximation would only slightly affect the change in the total energy, since the change in the Fermi energy would be affected in the opposite sense.

To get an expression for the total energy of the lattice, it is sufficient to take the total wave function of the electrons as a product of N one-electron wave functions; since the change in the correlation between electrons is being neglected. The total wave function is taken, therefore, as

$$\Psi = \psi_{\mathbf{k}_1}(\mathbf{r}_1)\ldots\psi_{\mathbf{k}_N}(\mathbf{r}_N),$$

where $\psi_{\mathbf{k}}$ denotes the one-electron wave function satisfying the equation

$$\nabla_i^2\psi_{\mathbf{k}}(\mathbf{r}_i) + [\epsilon_{\mathbf{k}} - \Sigma_a U_a(\mathbf{r}_i)]\psi_{\mathbf{k}}(\mathbf{r}_i) = 0,$$

and is normalized so that $\int|\psi_{\mathbf{k}}(\mathbf{r})|^2\,d\tau = 1$, over the sphere of radius L. $U_a(\mathbf{r}_i)$ is defined so that $U_a(\mathbf{r}_i) = V_a(\mathbf{r}_i)$, inside the polyhedron round ion a and is zero outside it. Using the Hamiltonian operator given in equation (2), we have

$$\int\ldots\int \Psi^*\Sigma_i H_0(\mathbf{r}_i)\Psi\,d\tau_1\ldots d\tau_N = \Sigma_{\mathbf{k}_i}\epsilon_{\mathbf{k}_i} + \Sigma_a\Sigma_i\int\psi^*_{\mathbf{k}_i}(\mathbf{r}_i)\{V_a(\mathbf{r}_i)-U_a(\mathbf{r}_i)\}\psi_{\mathbf{k}_i}(\mathbf{r}_i)d\tau_i.$$

The expression $\sum_i \int \psi^*_{\mathbf{k}_i}\{V_a - U_a\}\psi_{k_i} d\tau_i$ gives the potential energy of the charge distribution in the whole lattice except inside the a cell, due to the field of the ion a. Outside the a cell $V_a(\mathbf{r}) - U_a(\mathbf{r}) = -2/r_a$, where r_a is the distance to the ion a, and if the lattice is imagined to be divided into cells of equal volume Ω_a around each ion a, then

$$\sum_i \int \psi^*_{\mathbf{k}_i}\{V_a - U_a\}\psi_{k_i} d\tau_i = -\sum_{b\neq a} \int_{\Omega_b} \frac{2}{r_a}\rho(\mathbf{r})\, d\tau,$$

where $\rho(\mathbf{r})$ is the charge density at the point $\mathbf{r}$. The part of the potential energy of the lattice due to the electrostatic interaction between the electrons is given by

$$\tfrac{1}{2}\sum_a \int_{\Omega_a}\int_{\Omega_a} \frac{2}{r_{12}}\rho(\mathbf{r}_1)\rho(\mathbf{r}_2)\, d\tau_1\, d\tau_2 + \sum\sum_{a\neq b} \int_{\Omega_a}\int_{\Omega_b} \frac{2}{r_{12}}\rho(\mathbf{r}_1)\rho(\mathbf{r}_2)\, d\tau_1\, d\tau_2.$$

The first term is the self energy of the charge distribution, and the second term is the mutual interaction energy of the set of polyhedra. Thus the expectation value of the total energy in the lattice can be written

$$\langle H\rangle = E_F + \sum_a w_a - \sum\sum_{a\neq b} \int_{\Omega_b} \frac{2}{r_a}\rho(\mathbf{r})\, d\tau + \sum\sum_{a\neq b} \int_{\Omega_a}\int_{\Omega_b} \frac{2}{r_{12}}\rho(\mathbf{r}_1)\rho(\mathbf{r}_2)\, d\tau_1\, d\tau_2 + \sum\sum_{a\neq b} \frac{2}{r_{ab}},$$

where the last term arises from the interaction between the ions, $E_F = \sum_{\mathbf{k}_i} \epsilon_{\mathbf{k}_i}$ is the Fermi energy and $\sum_a w_a$ is the self energy of the charge distribution. Supposing that each cell can be replaced by a sphere within which the charge distribution is spherically symmetrical and $(1+q_a)$ is the total negative charge inside the a sphere, then it follows that

$$\langle H\rangle = E_F + \sum_a w_a + 2\sum\sum_{a\neq b}(q_a - q_b + q_a q_b)/r_{ab}. \qquad \ldots\ldots(21)$$

If a uniform charge distribution is assumed inside each a sphere, w_a will be equal to $(3/5)2r_0^{-1}q_a^2$ where r_0 is the radius of the sphere. The change in the total energy, when one atom of a pure metal is replaced by a foreign atom, is denoted by $\langle H\rangle - \langle H^{(0)}\rangle$, where $\langle H^{(0)}\rangle$ corresponds to a charge distribution with $q_a = 0$. $\langle H\rangle - \langle H^{(0)}\rangle$ is to be compared with $[\partial E/\partial c]_{c=0}$ obtained from the experimental values of the heat of solution (Ageew, Mansen and Sachs 1930).

The forms of the wave functions, obtained with the approximations of the present calculation, suggest that the excess q in the charge inside the central atomic sphere, is accompanied by a decrease q/N in the charge inside every other sphere. As it is difficult to calculate the exact charge distribution, the above distribution will be considered as a limiting case. The last term in (21) is then vanishingly small. For the solution of silver in copper the calculated value of $\langle H\rangle - \langle H^{(0)}\rangle$ is 0·0982 Rydberg units, while $[\partial E/\partial c]_{c=0} = 0{\cdot}0707$ Ryd., for the solution of copper in silver $\langle H\rangle - \langle H^{(0)}\rangle = -0{\cdot}0262$ Ryd., while $[\partial E/\partial c]_{c=0} = -0{\cdot}0324$ Ryd.

Another limiting case, in which the excess in the central charge is compensated by a decrease in the charge of the immediate neighbourhood, is suggested by the calculation of Huang (1948). The actual distribution of charge must be intermediate between these two cases. With this second assumption that only the

charge round each of the twelve nearest neighbours of the foreign atom is affected, it is found by direct calculation of (21) that $\langle H \rangle - \langle H^{(0)} \rangle$ is 0·0817 Ryd., when a silver atom is dissolved in a copper metal, and is −0·0439 Ryd., when a copper atom is dissolved in a silver metal.

The experimental values for the heats of solution of Ag in Cu and Cu in Ag are −7·2 and −6·8 kcal/mole respectively. The corresponding theoretical values, according to the above figures, are between −16·4 and −10·4 kcal/mole for the first case Ag in Cu and between −4·8 and −0·3 kcal/mole for the second case Cu in Ag. Although there is, therefore, no close agreement between the calculated and observed values of the heat of solution W, it should be remembered that W is obtained as the difference of two nearly equal quantities with the consequence that errors arising from the inevitable assumptions and approximations are greatly magnified. The fact that the theory leads to negative values of W and therefore to limited solubility in both cases is, in itself, of interest. It would be a searching test of the method, to apply it to the copper–gold system where the solid solutions are continuous. The reason this calculation has not already been made is that there appears to be no sufficiently accurate self-consistent field for gold yet available.

ACKNOWLEDGMENT

The writer wishes to express his indebtedness to Professor H. Jones for suggesting this problem and for his continuous advice and help throughout the work.

REFERENCES

Ageew, N., Mansen, M., and Sachs, G., 1930, *Z. Phys.*, **66**, 350.
Ageew, N., and Sachs, G., 1930, *Z. Phys.*, **63**, 293.
Black, M. M., 1934–1935, *Mem. and Proc., Manchester Lit. Phil. Soc.*, **74**, 32.
Grimm, H. G., and Wolff, H., 1934, *Handb. d. Phys.*, **24/2**, 1,073.
Hartree, D. R., 1933, *Proc. Roy. Soc.* A, **141**, 281.
Huang, K., 1948, *Proc. Phys. Soc.*, **60**, 161.
Jones, H., 1934, *Proc. Roy. Soc.* A, **144**, 225; 1937, *Proc. Phys. Soc.*, **49**, 243.

Mechanical Breakdown of a Non-Metallic Polycrystalline Material Observed by Reflected Light Microscopy *

By J. P. ROBERTS

High Temperature Materials Group, Metallurgy Department,
Royal Aircraft Establishment, Farnborough, Hants.

Communicated by L. G. Carpenter ; MS. received 20th October 1948

ABSTRACT. A study of fractures in a well-sintered polycrystalline aggregate of corundum crystals has shown that the strengths of the crystals and the crystal-boundaries are approximately equal. Reflected light microscopy was employed and the usefulness of this method of examination has been established.

§1. INTRODUCTION

A LOOSE-PACKED polycrystalline aggregate of corundum (α-alumina) crystals may be formed by slip-casting† or pressing. The specific gravity of such a mass is commonly 1·8–2·5, whilst that of a corundum single crystal is 4·0. If the aggregate be maintained for a few hours at 1,650–1,800° c. (melting point is 2,050° c.), some crystals grow at the expense of their neighbours and the process causes a diminution of the amount of void space and a corresponding increase in the specific gravity which may reach finally a value within 2% of that of the single crystal. The process is known as "sintering".

The mechanical strength of polycrystalline corundum bodies made in this way is a function of the temperature and duration of sintering. Before sintering, the aggregate is fragile and possesses negligible strength, but as sintering proceeds the strength increases, due to an increase in the strength of the bonding between the crystals and a reduction of the amount of void. Reliable information concerning the relative strengths of crystals and crystal-boundaries has been lacking. This paper describes a microscopical study of fractures in well-sintered corundum bodies; knowledge of the relative strengths has been gained.

Transmitted light examination was not adopted for observation of fractures, since, firstly, preparation of the necessary very thin sections in a plane perpendicular to a fracture is not fully satisfactory, due to the difficulty of avoiding loss of material during grinding, and, secondly, crystal-boundaries cannot always be discerned easily. Reflected light examination of this class of material has not been practised in the past, no doubt partly due to difficulties in polishing; corundum follows diamond on Mohs' Hardness Scale. A technique of polishing and etching sintered corundum was worked out for the fracture study.

Some observations concerning crystal-boundaries and etch-figures are included.

§2. EXPERIMENTAL PROCEDURE

Sintered corundum bars with crystal-size of approximately 100 μ were fractured in bend (stress in outermost fibres at fracture = 12–17 ton.in^{-2}, i.e. 1·9–2·6 × 10^9 dyne.cm^{-2}). The broken pieces were then fitted together, taking care that no parts of the fracture faces were damaged in this operation. After embedding in a suitable bakelite resin for ease of handling, a section was cut perpendicular to the plane of fracture.

* Crown copyright reserved. Reproduced with the permission of the Controller of H.M. Stationery Office.

† Slip-casting consists of pouring finely ground solid particles suspended in a suitable liquid medium into a porous mould, in which a cast is formed when the liquid is absorbed.

Plate I.

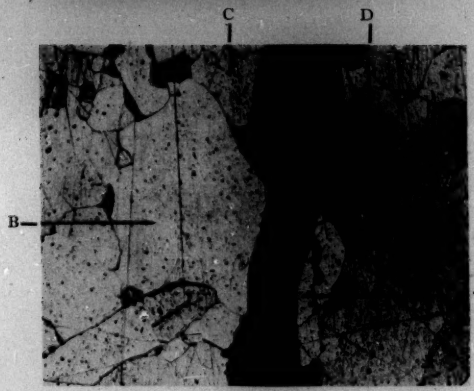

Plate II.

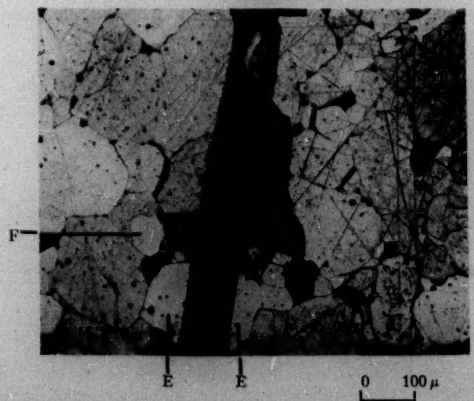

Plate III.

Fracture in a sintered aggregate of corundum crystals. (Magnification: 100×.)

To face page 249

The section was ground with silicon carbide particles of successively finer grades on a wet glass plate. The finest grit had a maximum particle size of 12 μ. The section was then polished in two stages; firstly, boron carbide (maximum particle size 6 μ) was employed on a pitch lap and, secondly, diamond dust (particle size range 4 to $<1\,\mu$) on a lead lap.

The polished section was etched by immersion in molten potassium hydrogen fluoride for approximately one minute.

The above procedure allowed study of that part of the fracture intersecting a plane cut through the interior of the bar. It was also desired to know the mode of fracture at the surface, for which purpose some bars were polished on their tension and compression faces, fractured, and etched afterwards.

The prepared sections were examined with the aid of an orthodox reflected light microscope using unpolarized light. The photomicrographs in Plates I–III are 100 times natural size.

The bars were made by slip-casting, the particle size being $<10\,\mu$ prior to sintering at 1,650° C. for 4 hours. The specific gravity was 3·80.

§3. RESULTS AND DISCUSSION

Plates I–III show interior sections of fractures. Transcrystalline failure has occurred at A–A, B–B, E–E. Shattering has caused removal of much material from other places adjacent to the fracture. The angular outlines of C, D (Plate II) suggest that they are parts of broken crystals. It is also considered that intercrystalline failure occurs, but evidence for this type is necessarily less definite than for transcrystalline failure. Study of twenty fractures strongly suggests that intercrystalline failure occurs in some cases. For instance, the irregular shape of the exposed perimeter of crystal F (Plate III) is more like a crystal-boundary than the types of transcrystalline failure observed.

No difference has been detected between the types of fracture occurring at the surface of and inside a bar.

Two types of transcrystalline failure may be distinguished; some fracture surfaces appear to be accurately planar, while others are curved. This is considered to depend upon whether the crystal has failed along a parting plane or has developed conchoidal fracture. Most writers on corundum agree that there is no true cleavage, but that crystals may sometimes be broken readily along {0001} basal and $\{10\bar{1}1\}$ rhombohedral planes (corundum is trigonal, class $\bar{3}$m). The phenomenon is called "parting"; in the case of the rhombohedral planes it is often attributed to polysynthetic twinning. If parting does not take place, corundum is said to fracture conchoidally. Crystals A–A, B–B, C, D appear to have failed conchoidally, whilst E–E appears to have parted.

Crystal-boundaries do not all show at the same stage of etching, so that when all are uncovered there is a divergence in the extents of attack at the different boundaries, as can be seen in the photomicrographs. Furthermore, the extent of attack frequently varies along the length of curved boundaries. It is considered that the extent to which a given boundary is attacked is a function of the difference between the orientations of the crystals forming the boundary and a function of the direction of the boundary. There is a connection here with recent work in metallurgy by Lacombe and Beaujard (1947), Lacombe (1948), and Forsyth, Metcalfe, King and Chalmers (1946), who have shown that the relative orientations of a grain boundary and the adjacent grains influence a number of phenomena, including etching,

boundary precipitation and "thermal etching". These studies are closely related to the grain-boundary transition-structure hypothesis of Gough (1927), Hargreaves and Hills (1929) and Chalmers (1937).

Well-formed etch-figures may be produced in the individual corundum crystals, provided that a planar polish of high quality is obtained and extreme care is taken during etching. A detailed study of the figures would no doubt provide useful information on the crystallographic orientations of the crystals which, in turn, would probably allow a closer investigation of the above-mentioned differential etching and perhaps lead to information about the mechanical strength of different types of boundary.

It is thought that the occurrence of trans- and intercrystalline failure at each point in a fracture face has been decided by one or both of two factors. Corundum crystals are anisotropic. The weaker planes within the crystal probably undergo fracture easily, whilst the stronger planes may be sufficiently strong to deflect the course of a fracture round the crystal-boundary. In this way the anisotropy of the crystals could account for the occurrence of simultaneous trans- and intercrystalline failure. A second factor which also would account for the experimental results is the non-uniformity of the boundaries, to which reference has already been made.

It is believed that reflected light examination of sintered corundum and other similar materials will prove to be superior to transmitted light examination for many studies, particularly those associated with crystal-boundaries. The author has used the technique to advantage in a study of bodies with high porosity.

§4. CONCLUSIONS

Since both trans- and intercrystalline failures occur when bars of well-sintered corundum are broken, it is concluded that the strengths of the crystals and the crystal-boundaries must be of comparable magnitudes. The results of experiments performed on large corundum single crystals, made by the Verneuil process and machined into bars, do not conflict with this conclusion. The bend strength of a single crystal is approximately equal to that of a well-sintered polycrystalline similar bar, suggesting that the crystal-boundaries are either as strong as or stronger than the crystals.

Reflected light examination of sintered corundum is not only possible but is in many respects superior to transmitted light examination, as, for example, in this type of investigation.

ACKNOWLEDGMENTS

Thanks are due to Mr. L. G. Carpenter for suggesting this study, to him and to Mr. W. Watt for their interest in its progress, and to Mr. A. R. Hall for assistance in the polishing. The author is indebted to the Chief Scientist, Ministry of Supply, for permission to publish.

REFERENCES

CHALMERS, B., 1937, *Proc. Roy. Soc.* A., **162**, 120.

FORSYTH, P. J. E., METCALFE, G. J., KING, R., and CHALMERS, B., 1946, *Nature, Lond.*, **158**, 875.

GOUGH, H. J., 1927, *Report of Discussion on Cohesion and Related Problems* (London: Faraday Society), p. 137.

HARGREAVES, F., and HILLS, R. J., 1929, *J. Inst. Metals*, **41**, 257.

LACOMBE, P., 1948, *Report of Conference on Strength of Solids* (London: Physical Society), p. 91.

LACOMBE, P., and BEAUJARD, L., 1947, *J. Inst. Metals*, **74**, 1.

The Measurement of the Rheological Properties of Visco-plastic Substances

By K. GOLDSMITH and J. IBALL *
Research Department, Lever Brothers & Unilever Ltd., Port Sunlight, Cheshire

MS. received 1*st June* 1948, *and in amended form* 11*th October* 1948

ABSTRACT. A torsion device is described in which a small and decreasing stress is exerted on the visco-plastic substance by means of a blade attached to a torsion wire. A modification of the Scott Blair-Nutting equation is suggested to account for the variation of both stress and strain with time and a " firmness intensity factor " of the substance is calculated, by means of the modified equation, from the observed relation between blade deflection and time. The apparatus has been used to study the properties of milk curds.

§1. INTRODUCTION

Much work has been published on the elasticity of gels, but little information is available on the region of plastic flow. The latter is particularly important for weak gels, where the elastic limit is easily exceeded, and where, therefore, the strength of the gel is primarily dependent on its visco-plastic properties. Measurements of such properties have been carried out hitherto on an empirical basis by cutting the gel by means of a specified knife or a plunger (Bloom 1924, Miller 1935) and thus subjecting it to an intensive local stress. This method has obvious limitations. Measurements under conditions of constant applied stress, which have been made on a number of plastic materials (Scott Blair and Coppen 1941, Broome and Bilmes 1941), and measurements of the shear force required to fracture gels (Hamer 1947), were found to present considerable experimental difficulties in the case of weak gels. Cheftel and Mocquard (1947) developed an apparatus for the recording of the deformation of gels under a varying applied force, but it did not permit evaluation of specific rheological properties. As a preliminary to the investigation of the visco-plastic properties of weak gels, therefore, a method of measuring their rheological properties was developed which is simple and free from some of the theoretical objections of the arbitrary methods. The method also permits determination of the viscosity of Newtonian liquids, and of the elasticity of Hookian solids, which may be considered as limiting cases of the visco-plastic state.

§2. APPARATUS

The rigidity of a material is found by observing the displacement under an applied force. The force should be exerted over an appreciable area, so that variations in the homogeneity of the materials are averaged out, and excessive local stresses are avoided. The most convenient way of applying a small stress is by means of a comparatively large blade attached to a fine torsion wire.

The construction of such a torsion apparatus is shown in Figure 1. A brass blade B is attached to a torsion wire W by means of a suitable clamping device. The wire is held by another clamp fixed to the torsion head H. Two pointers U and L are attached to the upper and lower clamps respectively. The apparatus

* Now at University College, Dundee.

is mounted on a retort stand so that the blade B can dip into a dish containing the substance, the firmness of which is to be measured. This dish is placed in a thermostatically controlled water bath.

If the upper pointer U is moved rapidly through a given angle between two adjustable stops, by turning the torsion head H, the blade B turns in the substance, and its deflection can be found by noting the position of pointer L on the scale S at given intervals of time. The rheological constants of the material can then be calculated from the relation between pointer deflection (in degrees) and time (in seconds), as described below.

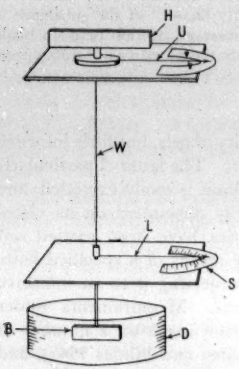

Figure 1. Diagram of torsion device.
H. Torsion head.
U. Upper pointer.
W. Torsion wire.
L. Lower pointer.
B. Blade.
S. Scale.
D. Glass dish.

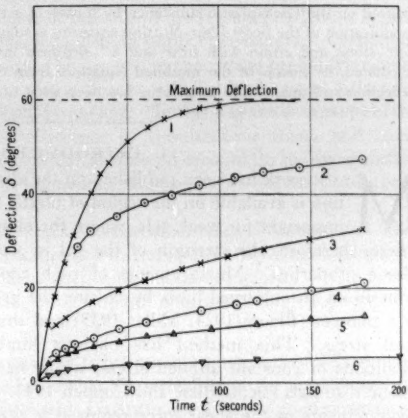

Figure 2. Relation between blade deflection (δ) and time (t) for oil and milk curds.
1. Polymerized castor oil ($\eta = 120$ poises).
2. Boiled milk (pH 5·02).
3. Full cream milk food (pH 5·3).
4. Pasteurized milk (pH 0·52).
5. Full cream milk food (pH 5·86).
6. Dried skimmed milk (pH 5·95).

The dimensions of the blade used were $1\frac{1}{2}$ in. $\times \frac{3}{8}$ in. $\times \frac{1}{16}$ in. The blade thickness is immaterial as long as the weight is sufficient to keep the torsion wire taut, but the inertia of the blade must be small compared with the retarding force exerted by the medium. If the diameter of the dish is not less than twice the length of the blade, no slipping of the substance occurs when the blade is turning. Tungsten and beryllium–copper are suitable metals for the torsion wire. The length and diameter of the wire depend on the maximum stress required. A 6 in. length of 40 S.W.G. tungsten wire, giving a maximum stress of 72 dynes/cm^2 with the $1\frac{1}{2}$ in. blade for torsion head deflections of 60°, was found to be suitable for the measurement of viscosities of the order of 100 poises.

§3. EXPERIMENTAL WORK

The present application of the torsion device was concerned primarily with the investigation of the properties of milk curd. This curd forms a weak gel with a low elastic limit. The properties of the gel vary with the acidity and the

type of the milk, and a wide range of different curds could thus be obtained. The curds were formed by coagulating an acidified 12·5% solution of milk powder by means of 0·45% solution of pepsin at 35° c. The torsion blade was inserted before the formation of the curd. Cutting by the blade destroys the structure of the curd, and a test cannot, therefore, be repeated on the same sample. This imposes some limitations on the reproducibility of the deflection–time curves where random variations from sample to sample occur, as was found to be the case with milk curds.

Curves of blade deflection against time for a vegetable oil and different milk curds are given in Figure 2, the maximum (torsion head) deflection being 60°. The readings of deflection were taken at intervals of ten seconds up to two minutes. Accurate readings could not be obtained below ten seconds because of the rapid initial movement of the blade. Some errors are also to be expected at the beginning of the deflection–time curve, owing to the impact of the blade on the medium.

§ 4. THEORETICAL TREATMENT

The deflection–time, δ–t, curve for oil, which is a Newtonian liquid, approaches the maximum deflection, i.e. the torsion head deflection α, logarithmically, and it can thus be expressed by the exponential relation

$$\alpha - \delta = \alpha \exp(-At) \qquad \ldots\ldots(1)$$

where A is a constant.

The curves for milk curd show that the deformation of these materials can be expressed neither independently of time, as in the case of Hookian solids, nor as an exponential function of time, which would indicate the viscous flow of a Newtonian liquid, and we are, therefore, dealing with "intermediate" materials of negligibly small elasticity.

Nutting (1921) and Scott Blair and Coppen (1940) have suggested an equation relating the shear strain σ of such materials to a power β of a constant shear stress S and also to a power k of the time of application t of the constant stress, so that

$$\sigma = S^{\beta} t^{k} / \Psi \qquad \ldots\ldots(2)$$

where Ψ is a constant of the material which may be described as the "firmness intensity factor".* This equation is not valid if both σ and S vary with t.

For the torsion device described above, S is not constant but varies with σ and thus with t. Several equations can be established to account for the variation of σ and S with t. Because of its simplicity, Scott Blair's equation for the rate of straining (Scott Blair 1944) is suggested in which the rate of change of σ with t is given by

$$d\sigma/dt = S_{(t)}^{\beta} k t^{k-1} / \Psi \qquad \ldots\ldots(3)$$

$S_{(t)}$ is the mean stress over the short time dt and is assumed constant during this time. This equation is applicable to the torsion device only, where the variation of σ and S with t are interdependent. It is equivalent to equation (2) when $S_{(t)}$ is constant.

For a viscous liquid, $\beta = 1$ and $k = 1$ and hence

$$d\sigma/dt = S_{(t)}/\Psi. \qquad \ldots\ldots(4)$$

Since

$$d\sigma/dt = d(dy/dx)/dt = dv/dx \qquad \ldots\ldots(5)$$

the velocity gradient dv/dx can be substituted in equation (4), which then becomes

* This term is used at the suggestion of Dr. G. W. Scott Blair.

Newton's equation of viscous flow with Ψ equal to the viscosity η. For an elastic solid, $\beta=1$ and $k=0$, so that $d\sigma/dt=0$. This represents the equilibrium condition between applied stress and reaction which will be set up almost instantaneously by the torsion blade, and is independent of time. Equation (3) is thus shown to be valid for two particular cases, and it may, therefore, be taken to be valid for any case intermediate between the elastic (solid) and the viscous (liquid) state.

Equation (3) can only be solved generally for σ if $S_{(t)}$ is specified. For a torsion wire of diameter D and length L twisted through an angle θ radians, the torque T is given by

$$T=\pi\theta D^4N/32L \qquad \ldots\ldots(6)$$

where N is the rigidity modulus of the material of which the wire is made.

The torque per degree twist, which is a constant for a particular wire, is therefore

$$G=\pi T/180\theta=\pi^2D^4N/5760L. \qquad \ldots\ldots(7)$$

If the torsion head is turned through an angle α, the torque at a blade deflection x is

$$T=G(\alpha-x) \qquad \ldots\ldots(8)$$

and the corresponding stress exerted on the substance to be tested is

$$S_{(t)}=4G(\alpha-x)/la \qquad \ldots\ldots(9)$$

where l is the length of the blade and a the total blade area. For a particular wire and blade arrangement,

$$S_{(t)}=C_1(\alpha-x) \qquad \ldots\ldots(10)$$

C_1 being a constant for the instrument.

It is more difficult to define the strain as there is certain to be some flow at the edges of the blade as the blade moves. But it is reasonable to define an element of strain as being proportional to an element of deflection, and hence

$$d\sigma=C_2dx. \qquad \ldots\ldots(11)$$

Substituting (10) and (11) in equation (3) and replacing the parameter t by the variable t_1, we obtain

$$dx/(\alpha-x)^\beta=C_1^\beta kt^{k-1}dt_1/\Psi C_2. \qquad \ldots\ldots(12)$$

Integrating between the limits $x=0$, $x=\delta$, $t_1=0$, $t_1=t$, where δ is the blade deflection at time t, this becomes

$$(\alpha-\delta)^{-(\beta-1)}-\alpha^{-(\beta-1)}=(\beta-1)C_1^\beta t^k/\Psi C_2. \qquad \ldots\ldots(13)$$

Equation (13) can be simplified when $\delta/\alpha\ll1$, so that

$$(1-\delta/\alpha)^{-(\beta-1)}\simeq1+(\beta-1)\delta/\alpha \qquad \ldots\ldots(14)$$

and, therefore, from equation (13),

$$\delta=(\alpha C_1)^\beta t^k/\Psi C_2. \qquad \ldots\ldots(15)$$

Writing, $\alpha C_1=C$, where C is an instrument constant, the "firmness intensity factor" Ψ is given by

$$\Psi=C^\beta t^k/\delta C_2. \qquad \ldots\ldots(16)$$

Equation (16) is expressed in logarithmic form as

$$\log\delta=\log(C^\beta/\Psi C_2)+k\log t. \qquad \ldots\ldots(17)$$

The relation between $\log\delta$ and $\log t$ should, therefore be linear. k, which is usually called the "dissipation coefficient", is given by the slope of this line. β is found for a given material by plotting $\log\delta - \log t$ lines for two experimental conditions, C' and C''. If the corresponding intercepts with the $\log\delta$ axis are B' and B'', then

$$\beta = (B' - B'')/\log(C'/C''). \qquad \ldots\ldots(18)$$

If $\beta = 1$, integration of equation (12) results in an equation

$$\ln\{\alpha/(\alpha-\delta)\} = C_1 t^k/\Psi C_2 \qquad \ldots\ldots(19)$$

or, taking logarithms and substituting $C_E = C_1/C_2$,

$$\log\ln\{\alpha/(\alpha-\delta)\} = \log(C_E/\Psi) + k\log t. \qquad \ldots\ldots(20)$$

The linear relation between $\log\ln(\alpha/(\alpha-\delta))$ and $\log t$ for the vegetable oil and for some milk curds is shown in Figure 3. The curves become inaccurate at short times for the reasons discussed above.

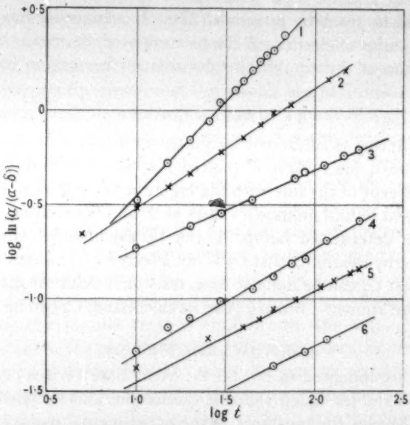

Figure 3. Relation between $\log\ln\alpha/(\alpha-\delta)$ and $\log t$ for oil and milk curds.

1. Polymerized castor oil.
2. Full cream milk food (pH 5·02).
3. Boiled milk (pH 5·02).
4. Modified milk food (pH 5·07).
5. Raw milk (pH 5·53).
6. Pasteurized milk (pH 6·0).

If $\delta/\alpha \ll 1$, $\ln\{\alpha/(\alpha-\delta)\} \simeq \delta/\alpha$, and equation (16) can also be applied to any material for which $\beta \simeq 1$. The use of a separate equation for the special case when $\beta = 1$ can thus be avoided. The relation between $\log\delta$ and $\log t$ can be expected to be linear where the relation between $\log\ln(\alpha/(\alpha-\delta))$ and $\log t$ is linear. The linearity of the curves given in Figure 3 is not dependent on the value of β.

For viscous liquids, $k = 1$ and Ψ becomes the viscosity η. Equation (19) can then be simplified, so that

$$\ln\{\alpha/(\alpha-\delta)\} = C_E t/\eta. \qquad \ldots\ldots(21)$$

If this equation is expressed as an exponential relation, it becomes

$$\alpha - \delta = \alpha \exp\{-(C_E/\eta)t\}. \qquad \ldots\ldots(22)$$

This is the same as equation (1), with $A = C_E/\eta$. It is thus shown that equation (3) is the general equation applicable where both σ and S vary with t, as is the case in the torsion apparatus described above.

For an elastic solid, $k = 0$ and Ψ becomes the modulus of elasticity E. Hence,

$$\ln\{\alpha/(\alpha - \delta)\} = C_E/E. \qquad \ldots\ldots(23)$$

Thus, the " firmness intensity factor " Ψ of a visco-plastic material can be found, where $\beta \neq 1$, from equation (16), and, where $\beta = 1$, from equation (19). It should be emphasized that in order to compare different materials it is not sufficient to give only values of Ψ. The values of k and β depend on the material and should be given in addition. The value of k, which lies between 0 and 1, indicates how far the material departs from a true liquid or from an elastic solid. Equation (16) can also be used where $\beta = 1$ if $\delta/\alpha \ll 1$. The viscosity η of a Newtonian liquid is given by equation (22). If a material has an appreciable elasticity, the modulus of elasticity E can be computed, by means of equation (23), from the deflection at the equilibrium position of the torsion blade for a given applied stress.

§ 5. CALIBRATION

The torsion device is calibrated by means of a liquid of known viscosity η. If a $\log \ln\{\alpha/(\alpha - \delta)\}$–$\log t$ curve is plotted for such a liquid, the ratio C_E/η is given by the intercept of the line with the $\log \ln\{\alpha/(\alpha - \delta)\}$ axis. C_E can then be calculated and used to find unknown values of Ψ or η from equations (19) or (22).

C_2 has to be determined before Ψ can be calculated from equation (16). This can be done by assuming that C_2 is not affected by changes of the constants Ψ, β and η, so that C_2 can be derived from tests on a different medium for which these constants are known. Since C_1 can be calculated, C_2 can be found from C_E.

ACKNOWLEDGMENTS

The authors are indebted to Dr. G. W. Scott Blair for his comments on this work, to Dr. V. Vand for much valuable discussion, and to Miss M. G. Watson and Mr. W. M. Morley for assistance in the experimental work.

REFERENCES

Bloom, W., 1924, *Ind. Eng. Chem.*, **16**, 310.
Broome, D. C., and Bilmes, L., 1941, *J. Soc. Chem. Ind.*, **60**, 184.
Cheftel, H., and Mocquard, J., 1947, *J. Soc. Chem. Ind.*, **66**, 297.
Hamer, W. J., 1947, *Bur. Stand. J. Res., Wash.*, **39**, 29.
Miller, D., 1935, *J. Dairy Sci.*, **18**, 259.
Nutting, F. G., 1921, *J. Franklin Inst.*, **191**, 629.
Scott Blair, G. W., 1944, *A Survey of General and Applied Rheology* (London : Pitman).
Scott Blair, G. W., and Coppen, F. M. V., 1940, *Nature, Lond.*, **146**, 840; 1941, *J. Soc. Chem. Ind.*, **60**, 190.

A Comparison of the Rates of Conditioning by Different Methods

By J. CRANK and M. E. HENRY
Courtaulds Limited, Maidenhead, Berks.

MS. received 7th September 1948

ABSTRACT. Four methods of conditioning a sample of material to a prescribed liquid or vapour content are examined mathematically. The " two-stage method " of conditioning leads to considerably shorter conditioning times than the other methods provided it is carried out in a certain way, and information presented in graphical form in this paper shows how to obtain the maximum advantage in practice. The necessary equations are developed for both a plane sheet and a cylinder, and the corresponding problem in heat flow is mentioned.

§ 1. INTRODUCTION

A common requirement, both in laboratory and industrial practice, is to cause a sample of material to absorb a prescribed amount of a given liquid or vapour, a process usually referred to as the "conditioning" of the sample. This frequently means that the sample is conditioned to be practically in equilibrium as regards its total content with a vapour of a given pressure, but there is sometimes the additional requirement that the distribution of liquid or vapour through the sample must have reached a prescribed degree of uniformity. The corresponding problem in heat flow is concerned with the conditioning of the sample to a uniform temperature. The problems are closely allied in that each is essentially a problem in diffusion, the first diffusion of matter and the second diffusion of heat, and the basic mathematical equations are the same in the two cases. The most obvious and simplest method of conditioning a sample to a vapour of given pressure is to suspend the sample in a bath or enclosure containing the vapour until the sample reaches equilibrium, the vapour pressure being maintained constant at the required value. In some cases, however, for example the conditioning of polymer films to water vapour or organic vapours at low pressures, the process is a slow one, and it is not uncommon for the time to condition satisfactorily to be as much as three or four weeks. It is therefore worth while to explore possible ways of reducing the time of conditioning. The present paper is concerned with a theoretical study of four ways of carrying out the conditioning process, and in particular with the calculation of optimum conditioning times for an ideal case in which conditioning is considered as a simple diffusion process in which the diffusion coefficient (or heat diffusivity) is assumed constant. Later in the paper, one example, in which the diffusion coefficient is assumed to increase linearly with concentration of diffusing substance, is included to indicate the general effect of non-constant diffusion or thermal properties and the extent to which the ideal calculations may be used as a guide to experimental procedure in a practical case.

The present discussion relates to diffusion of matter because the incentive to carry out the calculations described came from experimental work on diffusion in polymer films. The equations and general conclusions apply equally well to heat flow, though in that case uniform temperature distribution is nearly always the criterion of conditioning rather than the attaining of a prescribed total heat content.

§2. ALTERNATIVE METHODS OF CONDITIONING

Four different methods of carrying out the conditioning process are examined in this paper. They may be classified conveniently as (*a*) infinite bath conditioning; (*b*) two-stage conditioning; (*c*) finite bath conditioning; (*d*) insulated conditioning. The significance of each term needs some explanation.

(*a*) *Infinite Bath Conditioning*

This is the straightforward method referred to above in which the sample to be conditioned is immersed in a bath of vapour, the vapour pressure in the bath remaining constant at the value to which the sample is to be conditioned. The condition of constant vapour pressure is most readily secured by having a large amount of vapour in the bath compared with the amount finally taken up by the sample; theoretically this implies an infinite bath of vapour.

(*b*) *Two-stage Conditioning*

In this method two infinite baths of vapour are used, one at the pressure to which the sample is to be conditioned and the other at a higher vapour pressure. For convenience in discussion this will be referred to as saturated vapour though in practice it will be as high as practical considerations allow. The sample is first placed in the saturated vapour and after a certain time is transferred to the other bath and left to attain equilibrium. It will be shown that the success of this method depends on the time at which the transfer is carried out.

(*c*) *Finite Bath Conditioning*

If there is only a restricted amount of vapour, the vapour pressure in the bath decreases steadily as vapour is absorbed by the sample, the rate of fall being determined by the condition that the total amount of vapour in the bath and in the sample is conserved. If, for example, the vapour in the bath is initially saturated, the pressure can be made to approach the value to which the sample is to be conditioned by suitable adjustment of the respective volumes of bath and sample.

(*d*) *Insulated Conditioning*

The sample is again immersed in an infinite bath containing vapour at the highest convenient vapour pressure, and when the total content of the sample reaches the prescribed value the sample is removed from the bath and insulated by some means so that no further change in total content takes place while the desired degree of uniformity of concentration through the sample is approached. It will be seen that the same result can be achieved by causing the vapour pressure in the bath to vary in a particular way instead of insulating the sample.

§3. MATHEMATICAL SOLUTIONS FOR A PLANE SHEET

Subject to certain simplifying assumptions, calculations of the rate of conditioning by each of the above methods can be made. In this and the following two sections the sample is considered to have a geometric form such that it approximates to a solid of finite thickness bounded by two planes, e.g. a disc the area of whose edge is negligible compared with the area of the plane faces, so that conditioning may be considered to take place by diffusion in one dimension only, normal to the plane faces. The diffusion coefficient (or heat diffusivity) is assumed constant. In treating the finite bath problem it is also necessary to assume Henry's law of solubility in order to obtain formal solutions of the mathematical equations. For

conditioning by the other methods, a knowledge of the absorption isotherm may be necessary in order to apply the methods in a practical case but it is not necessary for the mathematical treatment presented here, and the isotherm need not be a linear one. Since the liquid or vapour to which the sample is to be conditioned may be either a complete solvent or only a swelling agent for the sample, it is convenient to refer to the diffusing substance by the general term "penetrant".

If C is the concentration of penetrant within the sample and D the constant diffusion coefficient, the basic equation, of which solutions are required for the boundary conditions corresponding to each of the four methods of conditioning, is

$$\frac{\partial C}{\partial t} = D\frac{\partial^2 C}{\partial x^2}. \qquad \ldots\ldots(1)$$

In the corresponding equation for heat flow C is replaced by temperature and D becomes the heat diffusivity given by $\kappa/\rho s$ where κ is heat conductivity, ρ the density, and s the specific heat of the sample. When the sample is immersed in an infinite bath it is supposed that the two surfaces of the sample reach a state of equilibrium with the vapour in the bath instantaneously, the concentration of penetrant just within each surface being related to the vapour pressure in the bath by the absorption isotherm. If the surface concentration of penetrant is denoted by C_0, a solution of (1) is required for the boundary conditions

$$C = C_0, \qquad x = 0, \qquad x = l, \qquad t \geqslant 0, \qquad \ldots\ldots(2)$$

and the initial condition

$$C = 0, \qquad 0 < x < l, \qquad t = 0, \qquad \ldots\ldots(3)$$

l being the thickness of the laminar sample. The solution is well known (Carslaw and Jaeger 1947) and is

$$C = C_0\left[1 - \frac{4}{\pi}\sum_{m=0}^{\infty}\frac{1}{2m+1}\sin\frac{(2m+1)\pi x}{l}\exp\left\{\frac{-D(2m+1)^2\pi^2 t}{l^2}\right\}\right]. \qquad \ldots\ldots(4)$$

The total amount of penetrant M_t absorbed by the sample at time t is given by integrating (4) with respect to x, i.e. $M_t = \int_0^l C(x', t)\,dx'$, and it is easily shown that

$$M_t = C_0 l\left[1 - \frac{8}{\pi^2}\Sigma\frac{1}{(2m+1)^2}\exp\left\{\frac{-D(2m+1)^2\pi^2 t}{l^2}\right\}\right]. \qquad \ldots\ldots(5)$$

The first part of two-stage conditioning, prior to transfer to the second bath, is also governed by equations (4) and (5), with C_1 substituted for C_0 if C_1 is the constant concentration of penetrant just within the surfaces of the sample in the first bath. At the time of transfer, say t_1, there will be some sort of non-uniform distribution of concentration through the sample so that diffusion in the second bath is subject to conditions of the form

$$C = C_2 = \text{constant}, \qquad x = 0, \qquad x = l, \qquad t \geqslant t_1, \qquad \ldots\ldots(6)$$

$$C = f(x), \qquad 0 < x < l, \qquad t = t_1, \qquad \ldots\ldots(7)$$

and in general the solution of (1) for conditions (6), (7), is

$$C = C_2\left[1 - \frac{4}{\pi}\sum_{r=0}^{\infty}\frac{1}{2r+1}\sin\frac{(2r+1)\pi x}{l}\exp\left\{\frac{-D(2r+1)^2\pi^2(t-t_1)}{l^2}\right\}\right]$$
$$+ \frac{2}{l}\sum_{n=1}^{\infty}\sin\frac{n\pi x}{l}\exp\left\{\frac{-Dn^2\pi^2(t-t_1)}{l^2}\right\}\int_0^l f(x')\sin\frac{n\pi x'}{l}\,dx'. \qquad \ldots\ldots(8)$$

This can be simplified in the present context because $f(x)$ represents the concentration distribution in the sample at the end of the first stage of two-stage conditioning, i.e. it is the result of immersion in an infinite bath of concentration C_1 for a time t_1. $f(x)$ is thus given by substituting the values $t=t_1$, $C_0=C_1$ in (4). In this case it is easy to show that

$$\int_0^l f(x')\sin\frac{n\pi x'}{l}\,dx' = \frac{2lC_1}{(2r+1)}\left[1-\exp\left\{\frac{-D(2r+1)^2\pi^2 t_1}{l^2}\right\}\right], \quad \ldots\ldots(9)$$

where $(2r+1)$ is written for odd n, so that the course of conditioning in the second stage is determined by the equation

$$C=C_2\left[1-\frac{4}{\pi}\sum_{r=0}^{\infty}\frac{1}{2r+1}\sin\frac{(2r+1)\pi x}{l}\exp\left\{\frac{-D(2r+1)^2\pi^2(t-t_1)}{l^2}\right\}\right]$$
$$+\frac{4C_1}{\pi}\sum_{r=0}^{\infty}\frac{1}{2r+1}\sin\frac{(2r+1)\pi x}{l}$$
$$\times\left[1-\exp\left\{\frac{-D(2r+1)^2\pi^2 t_1}{l^2}\right\}\right]\exp\left\{\frac{-D(2r+1)^2\pi^2(t-t_1)}{l^2}\right\}. \quad \ldots\ldots(10)$$

The integrated form of (10) is

$$M_t=C_2 l\left[1-\frac{8}{\pi^2}\sum_{r=0}^{\infty}\frac{1}{(2r+1)^2}\exp\left\{\frac{-D(2r+1)^2\pi^2(t-t_1)}{l^2}\right\}\right]+\frac{8C_1 l}{\pi^2}\sum_{r=0}^{\infty}\frac{1}{(2r+1)^2}$$
$$\times\left[1-\exp\left\{\frac{-D(2r+1)^2\pi^2 t_1}{l^2}\right\}\right]\exp\left\{\frac{-D(2r+1)^2\pi^2(t-t_1)}{l^2}\right\}. \quad \ldots\ldots(11)$$

The problem of the finite bath may be formulated mathematically as follows. Suppose the sample, of thickness l, occupies the space $-\frac{1}{2}l\leqslant x\leqslant\frac{1}{2}l$, while the bath, of limited extent, occupies the spaces $-\frac{1}{2}(l+h)\leqslant x\leqslant-\frac{1}{2}l$, $\frac{1}{2}l\leqslant x\leqslant\frac{1}{2}(l+h)$. The concentration in the sample is initially zero, and in the bath is always uniform. Let the partition factor k denote the ratio of the concentration in the sample to that in the bath when a state of equilibrium is reached, and C_1 denote the initial surface concentration just within the sample. Then the initial uniform concentration in the bath is C_1/k. It is assumed that the surface concentration just within the sample is always k times the uniform concentration in the bath throughout the conditioning. Taking $C(x,t)$ for the concentration of penetrant in the sample as before, the total amount of penetrant in the sample at time t is $2\int_0^{\frac{1}{2}l} C(x',t)\,dx'$, and so the boundary condition on the surface $x=\frac{1}{2}l$, expressing conservation of penetrant is

$$hC/k+2\int_0^{\frac{1}{2}l} C\,dx=hC_1/k, \qquad x=\tfrac{1}{2}l, \qquad t\geqslant 0. \quad \ldots\ldots(12)$$

The initial condition is

$$C=0, \qquad -\tfrac{1}{2}l\leqslant x\leqslant\tfrac{1}{2}l, \qquad t=0. \quad \ldots\ldots(13)$$

A convenient solution of the diffusion equation, subject to conditions (12), (13), takes the form

$$C=C_\infty\left\{1+2\sum_{n=1}^{\infty}\exp(-Dq_n^2 t)\frac{1+\alpha}{1+\alpha+\alpha^2 q_n^2}\frac{\cos(2q_n x/l)}{\cos q_n}\right\}, \quad \ldots\ldots(14)$$

where the q_n's are the non-zero positive roots of $\tan q_n = -\alpha q_n$; α, the parameter expressing the finiteness of the bath, is given by $\alpha = h/(kl)$; C_∞ is the uniform concentration in the sample attained theoretically after infinite time and $C_\infty = \alpha C_1/(1+\alpha)$. The integrated form of (14) is

$$\frac{M_t}{M_\infty} = 1 - \sum_{n=1}^{\infty} \frac{2\alpha(\alpha+1)}{1+\alpha+\alpha^2 q_n^2} \exp(-Dq_n^2 t), \qquad \ldots\ldots(15)$$

where M_∞ is the amount of penetrant in the sample after infinite time and is related to the other parameters by $M_\infty = C_1 h/k(1+\alpha)$. The solution (15) was derived by A. H. Wilson (1948) and (14) follows readily from the equations of his paper.

The process of conditioning by the fourth method prior to insulation is again governed by equations (4) and (5) for the infinite bath. The condition that the sample is insulated after a certain time t_2 is simply that $\partial C/\partial x = 0$, $x = 0$, $x = l$, $t \geqslant t_2$. The solution of the diffusion equation for a plane sheet insulated on both surfaces and with the initial condition $C = f(x)$, $0 < x < l$, $t = t_2$, is (Carslaw and Jaeger 1947)

$$C = \frac{1}{l}\int_0^l f(x')\,dx' + \frac{2}{l}\sum_{n=1}^{\infty} \exp\left\{\frac{-Dn^2\pi^2(t-t_2)}{l^2}\right\} \cos\frac{n\pi x}{l} \int_0^l f(x') \cos\frac{n\pi x'}{l}\,dx'. \qquad \ldots\ldots(16)$$

In the present example $f(x)$ is given by evaluation of (4) at the time $t = t_2$, with C_1 written for C_0 if the infinite bath used prior to insulation is taken to have the same concentration as that used in the first stage of two-stage conditioning. It can readily be shown that the two integrals of (16) then reduce respectively to

$$\int_0^l f(x')\,dx' = C_1 l\left[1 - \frac{8}{\pi^2}\sum_{m=0}^{\infty} \frac{1}{(2m+1)^2} \exp\left\{\frac{-D(2m+1)^2\pi^2 t_2}{l^2}\right\}\right], \qquad \ldots\ldots(17)$$

and

$$\int_0^l f(x') \cos\frac{2p\pi x'}{l}\,dx' = \frac{8C_1 l}{\pi^2}\sum_{m=0}^{\infty} \frac{1}{4p^2-(2m+1)^2} \exp\left\{\frac{-D(2m+1)^2\pi^2 t_2}{l^2}\right\}, \qquad \ldots\ldots(18)$$

where $2p$ is substituted for n since only the terms involving even n are non-zero. The property of particular interest is the variation of surface concentration with time after insulation, and this is given by evaluation of (16) at $x = 0$, having substituted from (17) and (18) for the integrals. We have finally,

$$\frac{C_{x=0}}{C_1} = 1 - \frac{8}{\pi^2}\sum_{m=0}^{\infty} \frac{1}{(2m+1)^2} \exp\left\{\frac{-D(2m+1)^2\pi^2 t_2}{l^2}\right\} + \frac{16}{\pi^2}\sum_{p=1}^{\infty}\sum_{m=0}^{\infty} \frac{1}{4p^2-(2m+1)^2} \exp\left\{\frac{-4Dp^2\pi^2(t-t_2)}{l^2}\right\} \exp\left\{\frac{-D(2m+1)^2\pi^2 t_2}{l^2}\right\}. \qquad \ldots\ldots(19)$$

Equation (19) expresses the way in which the concentration at the surface of the sheet varies after insulation, the total content of the sample remaining unchanged. As an alternative to insulation if the surface concentration is caused to vary by some external means, in accordance with (19), after the time t_2, the effect will be identical with insulation, the surface gradient of concentration remaining constant and zero, and the sample neither gaining nor losing penetrant.

§4. NUMERICAL COMPARISON OF THE FOUR METHODS OF CONDITIONING

In order to see whether the time of conditioning differs appreciably in the different methods, some of the above solutions have been evaluated numerically. Since it is only after infinite time that a sample is completely conditioned to the extent of having a perfectly uniform concentration throughout, some arbitrary criterion of a conditioned sample must be adopted. A sample will be said to be conditioned with respect to its total content at a time when the content differs by $\pm 1\%$ from the ideal value it would reach after infinite time, provided it never deviates by more than $\pm 1\%$ from the ideal value at any subsequent time. The distribution of concentration through the sample at the time of conditioning, as just defined, is examined later.

The constant concentration just within the surface of the sheet in the first part of two-stage conditioning has been denoted by C_1 and it is convenient to use this as a unit of concentration. The corresponding total content of the sample, after immersion for an infinite time in an infinite bath such that the surface concentration is C_1, is lC_1, which is a convenient unit in which to measure total content of penetrant in the sample at any time. Thus on this scale, the total content of the sample will approach unity if left in the first stage bath of two-stage conditioning for an infinite time. The non-dimensional unit of time Dt/l^2 is used as usual. Figure 1 shows the progress of conditioning to a total content of $\frac{1}{3}C_1$ in an infinite bath for which the surface concentration is $\frac{1}{3}C_1$, and also by two-stage conditioning. The curve shown for the infinite bath is obtained by evaluating (5) for $C_0 = \frac{1}{3}C_1$, and the curves for two-stage conditioning by evaluating (5) for $C_0 = C_1$ and (11) for $C_2 = \frac{1}{3}C_1$. A number of curves are drawn corresponding to different times of transfer t_1 from the first bath to the second. The four values of time of transfer are given by $Dt_1/l^2 = 0{\cdot}012$, $0{\cdot}025$, $0{\cdot}040$, $0{\cdot}060$ respectively. The curve corresponding to transfer after the shortest time shows a minimum, the total content of the sample first decreasing after transfer and then increasing and approaching equilibrium at a time not much different from that shown by the infinite bath solution. The curve for which $Dt_1/l^2 = 0{\cdot}025$ has a similar behaviour. The sample left in the first bath for the longest time contains an excess of penetrant at the time of transfer, and after transfer the total content steadily decreases reaching the 101% limit only a short time before the infinite bath solution reaches the 99% limit. Figure 1 shows, however, that there is an optimum time of transfer at about $Dt_1/l^2 = 0{\cdot}040$, for which the conditioning curve reaches the 101% limit much sooner than any of the others, and which remains within the limits of $\pm 1\%$ thereafter. This optimum curve has a minimum at 99% of the equilibrium content. In Figure 2 the optimum curve for two-stage conditioning is compared with the infinite bath curve and with the finite bath curve calculated from equation (15) with $\alpha = \frac{1}{2}$, the initial surface concentration in the finite bath being C_1, the same as in the first bath for two-stage conditioning. The finite bath method leads to quicker conditioning than the infinite bath, but is slower than the optimum two-stage conditioning. Thus the times of conditioning by two stage, finite bath and infinite bath methods in this example are given by $Dt/l^2 = 0{\cdot}062$, $0{\cdot}200$, $0{\cdot}450$ respectively. If the two-stage conditioning is prolonged till the 99% limit is reached, to be more strictly comparable with the other two, the time $0{\cdot}062$ is to be replaced by $0{\cdot}090$, so that two-stage conditioning represents an improvement on infinite bath conditioning by a factor of five or more in this particular case.

It might be expected that the transferring of the sample from one bath to another at a different concentration in two-stage conditioning would produce a non-uniform distribution of concentration within the sample which may persist from some time after the transfer, so that, even when the sample is satisfactorily conditioned as regards its total content, it may not have achieved the desired degree of uniformity of concentration. Figure 3 shows concentration–distance curves obtained by evaluating (10) for $C_2=\frac{1}{3}C_1$ for the times at which M_t/lC_1

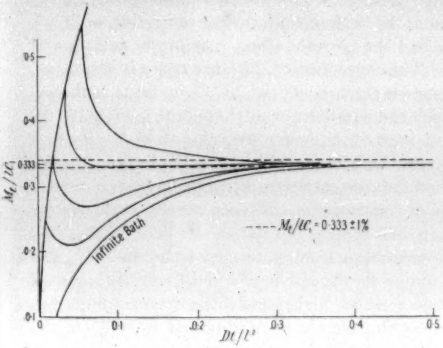

Figure 1. Two-stage conditioning of a plane sheet $C_2=\frac{1}{3}C_1$.

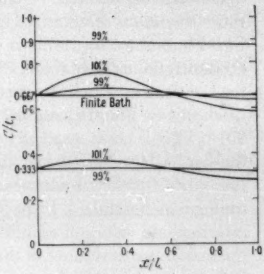

Figure 3. Concentration—distance curves for a plane sheet.

The figures 99% and 101% refer to the total content of the sheet at the times for which the curves are drawn, expressed as a percentage of the equilibrium content.

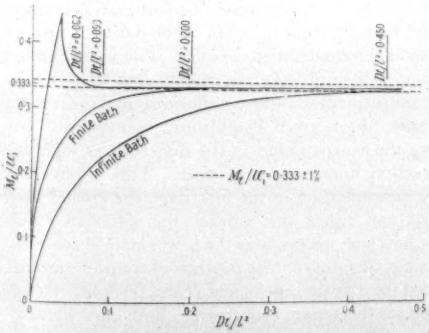

Figure 2. Comparison of methods of conditioning of a plane sheet $C_2=\frac{1}{3}C_1$.

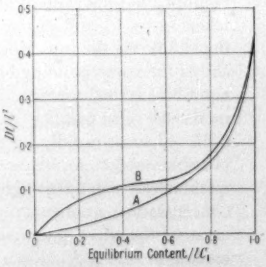

Figure 4. Conditioning and transfer times for a plane sheet.

A. Time of transfer.
B. Time to reach 99% equilibrium content.

reaches 101% and 99% of the final equilibrium value of $\frac{1}{3}lC_1$. At the earlier time the concentration is appreciably non-uniform, the maximum deviation from the desired concentration of $C/C_1=\frac{1}{3}$ being about 10%. By the time the total content has fallen to the 99% limit, however, the concentration is as uniformly distributed as it would be after conditioning to 99% in an infinite bath, the concentration distance curves being indistinguishable on the diagram.

Corresponding calculations for conditioning to different total contents lead to qualitatively similar results as regards the overall rate of absorption curves. In each case there is one time of transfer in the two-stage method which leads to a substantially shorter time of conditioning than is achieved by finite or infinite bath methods. It is not possible to show all the results in detail but in Figure 3 concentration–distance curves are shown for cases in which the total content of the sample is conditioned to $2lC_1/3$ and $9lC_1/10$ in addition to $\frac{1}{3}lC_1$ already discussed. When the total content reaches 101% of $2lC_1/3$, the concentration shows a maximum deviation of about 14% from the desired uniform concentration of $2C_1/3$, but when the 99% limit is reached the corresponding maximum deviation of concentration is only about 3%. The concentration–distance curve is also shown for the time at which the total content reaches 99% of $2lC_1/3$ by finite bath conditioning. For the case in which the equilibrium total content is $9lC_1/10$, the 101% limit is never attained in two-stage conditioning, the value of M_t/lC_1 at which the sample is transferred to the second bath lying within the $\pm 1\%$ limits. In this case when the 99% limit is reached the concentration distribution is seen to be as uniform as possible. Inspection of concentration–distance curves, evaluated for intermediate values of equilibrium total content but not shown here, reveals that the maximum deviations of the concentration from uniformity when the 101% and 99% limits are reached are most serious for the case in which the equilibrium total content is $2lC_1/3$; the deviations decrease for higher and lower total contents and so in two-stage conditioning, when the sample is conditioned to 99% of the equilibrium total content, the greatest deviation of concentration at any point in the sample from the desired uniform value is never greater than about 3%.

In Figure 4, the lower curve shows the way in which the optimum time of transfer from the first bath to the second in two-stage conditioning depends on the equilibrium total content desired, i.e. the concentration in the first bath is always taken to be C_1 and in the second bath the concentration takes different values depending on the prescribed state of the conditioned sample. The upper curve shows the corresponding behaviour of the time taken to condition to 99% of the equilibrium total content. Both times increase as the equilibrium total content is increased. In practice this means that a given equilibrium content will be achieved most rapidly by making the concentration in the first bath as high as possible subject to whatever practical limitations may exist. This is obvious qualitatively since the higher the concentration in the first stage the greater the concentration gradients involved and hence the quicker the diffusion. To estimate the effect quantitatively, however, necessitates the mathematical analysis leading to Figure 4. For a given equilibrium content the time of transfer may be read from the lower curve provided the diffusion coefficient D and thickness of the sample are known or can be found for the system concerned. Both curves reach the value $Dt/l^2 = 0{\cdot}45$ when the equilibrium content is lC_1 since we then have conditioning by the infinite bath method arising as a special case of two-stage conditioning. The effect of making the concentration in the first bath high relative to that in the second bath is also to produce a more uniform distribution of concentration through the sample at the time of conditioning as previously shown by Figure 3, provided the desired equilibrium content is less than $2lC_1/3$.

For practical purposes in two-stage conditioning it may sometimes be more convenient to know the value of the total content of the sample at which the transfer is to be made rather than the time of transfer, i.e. to know M_t/lC_1 at time t_1 instead

of t_1 itself. In Figure 5 the excess absorption at the time of transfer is plotted as a function of the equilibrium total content. Excess absorption is the amount by which the total content of the sample at the time of transfer exceeds the desired final equilibrium content. This excess is necessarily zero at each end of the curve, i.e. for equilibrium content zero and lC_1, and the curve passes through a maximum value for an equilibrium content of about $0{\cdot}16lC_1$, where the excess absorption is $0{\cdot}146lC_1$. For equilibrium contents higher than that at which the maximum occurs the relation plotted in Figure 5 is closely linear. Thus if the total amount of penetrant in the sample can be measured by some means as conditioning proceeds, Figure 5 may be used to determine, for a prescribed equilibrium content, what the content of the sample should be when it is transferred from the first to the second bath in order to secure optimum two-stage conditioning.

Reference to Figure 1 shows that if the sample is left in an infinite bath such that the concentration just within the surface of the sample is constant at C_1, the amount of penetrant in the sample reaches the value $\frac{1}{3}lC_1$ when $Dt/l^2 = 0{\cdot}025$. If the sample is insulated at this time the total content remains fixed and the surface

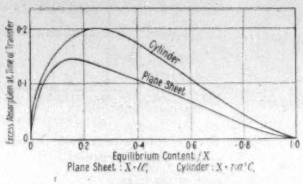

Figure 5.

For the plane sheet excess absorption is the difference between M_t/lc_1 at the time of transfer and at equilibrium.
For the cylinder excess absorption is the difference between $M_t/\pi a^2 C_1$ at the time of transfer and at equilibrium.
In each case M_t is the content of the sample at time t.

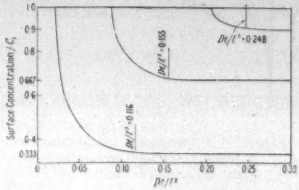

Figure 6. Insulated conditioning of a plane sheet.

The values of Dt/l^2 indicated are those at which the surface concentration falls to within 1% of its equilibrium value.

concentration falls according to equation (19). The complete time variation of surface concentration is shown in Figure 6, for equilibrium contents $\frac{1}{3}lC_1$, $2lC_1/3$ and $9lC_1/10$. The times taken for the surface concentration to fall to within 1% of its equilibrium value are indicated, and comparison with Figure 4 shows these times to be slightly greater than the corresponding times to condition to 99% equilibrium content by two-stage conditioning. Instead of insulating the sample the same result can be achieved by causing the concentration in the bath to vary in such a way that the surface concentration of the sample behaves acccording to the curves of Figure 6. Since the steady state is approached at approximately the same rate as in the two-stage conditioning, this method may in some cases prove a useful alternative to the two-stage method.

§5. EFFECT OF VARIABLE DIFFUSION OR THERMAL PROPERTIES

The above mathematical solutions and discussion are based on the assumption that the diffusion coefficient, or thermal properties in the case of heat flow, are constant. There are many systems, however, for which this assumption is not justified, but where, for example, the diffusion coefficient varies considerably with concentration of penetrant. This is frequently the case when water vapour or

organic vapours or liquids diffuse into polymer sheets, though there is a lack of accurate measurements of the concentration dependence. When the diffusion coefficient is dependent on concentration it is no longer possible to write down formal mathematical solutions of the diffusion equation but a numerical solution can be obtained for each particular case. To illustrate in a general way the effect on the rate of conditioning of a diffusion coefficient which increases with increasing concentration of penetrant, a solution has been evaluated by a numerical process of integration (Crank and Nicolson 1947) for a diffusion coefficient D given by $D = D_0(1 + 10C/C_1)$ where D_0 is constant and C and C_1 have the same significance as in § 4. In Figure 7 the curves for infinite bath and two-stage conditioning for this

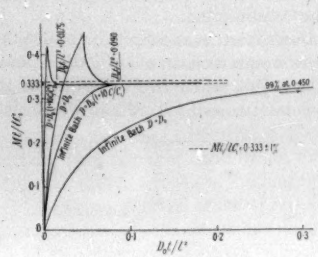

Figure 7. Two-stage conditioning of a plane sheet for variable and constant diffusion coefficients.

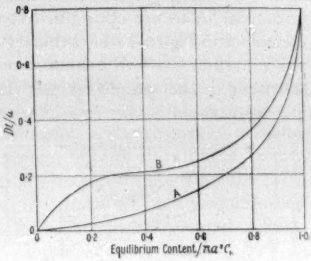

Figure 8. Conditioning and transfer times for a cylinder.

A. Time of transfer.
B. Time to reach 99% equilibrium.

variable D are compared with the corresponding curves for a constant coefficient $D = D_0$, taken from Figure 2, for the case in which the equilibrium content of the sample is $\frac{1}{3}lC_1$. Both methods lead to quicker conditioning for the variable diffusion coefficient than for the constant one, and furthermore, the advantage of using the two-stage method is slightly enhanced when D increases with increasing concentration of penetrant. Thus the ratio of the times of conditioning to the 99% limit by the two methods is 5·14 when $D = D_0(1 + 10C/C_1)$ and 5·00 when $D = D_0$. It can easily be seen from general reasoning that the effect of a diffusion coefficient increasing with concentration must be qualitatively in this direction, since the average value of D is greater than D_0 and so both methods of conditioning must be quicker. Furthermore, the effect of using a high concentration in the first bath means that the relatively high values of D at high concentrations are allowed to influence the rate of conditioning, whereas in the infinite bath method concentrations above $\frac{1}{3}C_1$ do not appear. In general therefore in a system in which the diffusion coefficient increases with increasing concentration the advantage gained by using two-stage conditioning is even greater than is indicated by the results for a constant coefficient presented in § 4.

When $D = D_0(1 + 10C/C_1)$ the excess absorption at the time of transfer does not differ greatly in the example considered from the corresponding excess when $D = D_0$, being about 0·092 in one case and 0·117 in the other. This suggests that in many cases, even though the diffusion coefficient is variable the mathematical solutions for a constant diffusion coefficient will be a useful guide to the amount of penetrant which the sample should contain when transferred from the first bath

to the second. In other cases, of course, it may be necessary to explore the system to find the optimum time of transfer, either by carrying out the process of numerical solution of the differential equation for the appropriate form of diffusion coefficient, if this is known, or by practical trial and error.

§ 6. CONDITIONING OF A CYLINDRICAL SAMPLE

The four different methods of conditioning can of course be used if the sample approximates to the form of an infinitely long circular cylinder of radius a. The general reasoning is precisely as for the plane sheet and the appropriate formulae for the cylinder will be presented with a minimum of explanation.

The basic equation for radial diffusion in a cylinder is

$$\frac{\partial C}{\partial t} = \frac{D}{r}\frac{\partial}{\partial r}\left(r\frac{\partial C}{\partial r}\right). \qquad \ldots\ldots(20)$$

In the infinite bath, taking C_0 as before for the concentration of penetrant just within the surface of the cylinder, the required solution of (20) is (Carslaw and Jaeger 1947)

$$C = C_0\left\{1 - 2\sum_{m=1}^{\infty}\frac{J_0(q_m r/a)}{q_m J_1(q_m)}\exp\left(-Dq_m^2 t/a^2\right)\right\}, \qquad \ldots\ldots(21)$$

when the initial concentration throughout the cylinder is zero. q_m is the mth root of the equation $J_0(q_m) = 0$. The integrated form of (21) is

$$M_t = \pi a^2 C_0\left\{1 - 4\sum_{m=1}^{\infty}\frac{1}{q_m^2}\exp\left(-Dq_m^2 t/a^2\right)\right\}. \qquad \ldots\ldots(22)$$

The first part of two-stage conditioning is governed by equations (21), (22) with C_1 substituted for C_0 if C_1 is the concentration of penetrant at the surface of the cylinder in the first bath. Diffusion in the second bath is subject to the conditions

$$C = C_2 = \text{constant}, \qquad r = a, \qquad t \geqslant t_1, \qquad \ldots\ldots(23)$$

$$C = f(r), \qquad 0 < r < a, \qquad t = t_1, \qquad \ldots\ldots(24)$$

where t_1 is the time of transfer from the first bath to the second, and in general the solution of (20) with (23), (24) is

$$C = C_2\left\{1 - 2\sum_{n=1}^{\infty}\frac{J_0(q_n r/a)}{q_n J_1(q_n)}\exp\left\{-Dq_n^2(t-t_1)/a^2\right\}\right\} + \frac{2}{a^2}\sum_{n=1}^{\infty}\exp\left\{-Dq_n^2(t-t_1)/a^2\right\}\frac{J_0(q_n r/a)}{\left\{J_1(q_n)\right\}^2}\int_0^a r' f(r') J_0(q_n r'/a)\,dr', \qquad \ldots\ldots(25)$$

where $J_0(q_n) = 0$ now.

For the particular case where $f(r)$ is given by substituting $t = t_1$, $C_0 = C_1$ in (21), we find

$$\int_0^a r' f(r') J_0(q_n r'/a)\,dr' = C_1 a^2\{1 - \exp\left(-Dq_n^2 t_1/a^2\right)\} J_1(q_n)/q_n, \qquad \ldots\ldots(26)$$

and (25) becomes

$$C = C_2\left\{1 - 2\sum_{n=1}^{\infty}\frac{J_0(q_n r/a)}{q_n J_1(q_n)}\exp\left\{-Dq_n^2(t-t_1)/a^2\right\}\right\} + 2C_1\sum_{n=1}^{\infty}\frac{J_0(q_n r/a)}{q_n J_1(q_n)}\left\{1 - \exp\left(-Dq_n^2 t_1/a^2\right)\right\}\exp\left\{-Dq_n(t-t_1)/a^2\right\}, \qquad \ldots\ldots(27)$$

of which the integrated form is

$$M_t=\pi a^2C_2\left\{1-4\sum_{n=1}^{\infty}\frac{1}{q_n^2}\exp\{-Dq_n^2(t-t_1)/a^2\}\right\}$$

$$+4\pi C_1a^2\sum_{n=1}^{\infty}\frac{1}{q_n^2}\exp\{-Dq_n^2(t-t_1)/a^2\}\{1-\exp(-Dq_n^2t_1/a^2)\}. \quad \ldots\ldots(27a)$$

For the finite bath problem we use cylindrical polar coordinates and assume the cylinder to occupy the space $r\leqslant a$, while the cross-section of the bath in which it is immersed is A, excluding the space occupied by the cylinder. The concentration in the cylinder is initially zero and in the bath is always uniform. The equation expressing the conservation of penetrant is

$$\frac{AC}{k}+2\pi\int_0^a rC\,dr=\frac{AC_1}{k}, \qquad r=a, \qquad t\geqslant 0, \qquad \ldots\ldots(28)$$

where C_1 is the initial concentration just within the cylinder surface and k is the partition factor for the penetrant in the sample and the bath as before. The required solution of (20) for these conditions is

$$C=C_\infty\left\{1+\sum_{n=1}^{\infty}\frac{4(1+\alpha)\exp(-Dq_n^2t/a^2)}{(4+4\alpha+\alpha^2q_n^2)}\frac{J_0(q_nr/a)}{J_0(q_n)}\right\}, \quad \ldots\ldots(29)$$

where the q_n's are the positive roots other than zero of $\alpha q_nJ_0(q_n)+2J_1(q_n)=0$, and $C_\infty=\alpha C_1/(1+\alpha)$, $\alpha=A/(\pi a^2k)$. The integrated form of (29) is (Wilson 1948)

$$\frac{M_t}{M_\infty}=1-\sum_{n=1}^{\infty}\frac{4\alpha(1+\alpha)}{4+4\alpha+\alpha^2q_n^2}\exp(-Dq_n^2t/a^2), \qquad \ldots\ldots(30)$$

where $M_\infty=C_1A/k(1+\alpha)$. The solution of (20) for a cylinder insulated at time t_2 and with the initial condition $C=f(r)$, $0<r<a$, $t=t_2$, is (Carslaw and Jaeger 1947)

$$C=\frac{2}{a^2}\left\{\int_0^a r'f(r')\,dr'+\sum_{n=1}^{\infty}\exp\{-Dp_n^2(t-t_2)/a^2\}\frac{J_0(p_nr/a)}{\{J_0(p_n)\}^2}\int_0^a r'f(r')J_0(p_nr'/a)\,dr'\right\}, \quad \ldots\ldots(31)$$

where the p_n's are the roots of

$$J_1(p_n)=0. \qquad \ldots\ldots(32)$$

If, prior to insulation, the concentration just within the surface of the cylinder is C_1, so that $f(r)$ is given by evaluation of (21) with $C_0=C_1$ and $t=t_2$, then it follows readily that

$$\int_0^a r'f(r')\,dr'=\tfrac{1}{2}C_1a^2\left\{1-4\sum_{m=1}^{\infty}\frac{1}{q_m^2}\exp(-Dq_m^2t_2/a^2)\right\}, \quad \ldots\ldots(33)$$

using the relation $\int_0^r r^{n+1}J_n(\beta r)\,dr=\beta^{-1}r^{n+1}J_{n+1}(\beta r)$. Also by using the relations

$$(\rho^2-\sigma^2)\int_0^a ruv\,dr=a\left[v\frac{du}{dr}-u\frac{dv}{dr}\right]_{r=a}, \quad u=J_n(\rho r), \quad v=J_n(\sigma r), \quad \ldots\ldots(34)$$

and the fact that, with (32), $\int_0^a rJ_0(p_nr/a)\,dr=0$, it can easily be shown that

$$\int_0^a r'f(r')J_0(p_nr'/a)\,dr'=\frac{2a^2C_1}{p_n^2-q_m^2}J_0(p_n), \qquad \ldots\ldots(35)$$

so that finally the concentration at the surface of the cylinder after insulation is given by

$$\frac{C_{r=a}}{C_1} = 1 - 4 \sum_{m=1}^{\infty} \frac{1}{q_m^2} \exp(-Dq_m^2 t_2/a^2) + 4 \sum_{n=1}^{\infty} \sum_{m=1}^{\infty} \frac{1}{p_n^2 - q_m^2} \exp\{-Dp_n^2(t-t_2)/a^2 \exp\}(-Dq_m^2 t_2/a^2). \quad \ldots\ldots(36)$$

By numerical evaluation of the mathematical solutions of this section the four methods of conditioning a cylindrical sample may be compared. The general behaviour of the overall rate of absorption and concentration–distance curves is closely similar to that of the corresponding curves for the plane sheet. For any given equilibrium content of the cylinder there is an optimum point of transfer from the first bath to the second in two-stage conditioning, which leads to a shorter conditioning time than that needed for finite bath conditioning, this latter being quicker than conditioning in an infinite bath. In insulated conditioning the surface concentration falls to within 1% of its equilibrium value in a time which is a little greater than the time of conditioning to 99% equilibrium content in two stages. The main features of practical interest for the cylindical sample are summarized in Figures 5 and 8. Figure 8 shows how the time of transfer and the time to condition to 99% of the equilibrium content by two-stage conditioning depend on the equilibrium content required, the concentration in the first bath being fixed. The upper curve in Figure 5 shows the excess absorption at the time of transfer as a function of equilibrium content. For a system in which the diffusion coefficient or thermal properties are constant the data of Figures 5 and 8 indicate how to carry out two-stage conditioning of a cylinder in order to achieve the optimum conditioning time.

§7. LIMITATIONS ON THE PRACTICAL APPLICATION OF THE MATHEMATICAL TREATMENT

All the mathematical solutions developed in this paper refer to the conditioning of a sample which is initially free from penetrant. The treatment could clearly be generalized, however, to cover cases in which the initial content is not zero.

A more serious restriction on the type of system to which the theoretical predictions may reasonably be expected to apply, arises out of the implicit assumption that there is no hysteresis in the vapour pressure–content isotherm. Thus comparing for example "infinite bath conditioning" with "two-stage conditioning", the former process is one of absorption only, whereas the latter is one of absorption followed by desorption. If the material shows hysteresis, the actual contents at the end of the two processes will be different, even though the vapour pressures are the same. These considerations limit the direct application of the treatment to systems in which hysteresis is not an important factor.

Somewhat similar restrictions will apply to the two-stage heat conditioning process if the material undergoes, at high temperatures, any physical change which is not entirely removed as the temperature falls again.

REFERENCES

CARSLAW, H. S., and JAEGER, J. C., 1947, *Conduction of Heat in Solids* (Oxford: Clarendon Press).

CRANK, J., and NICOLSON, P., 1947, *Proc. Camb. Phil. Soc.*, **43**, 50.

WILSON, A. H., 1948, *Phil. Mag.*, **39**, 48.

LETTERS TO THE EDITOR

A Travelling Wave Linear Accelerator with R.F. Power Feedback, and an Observation of R.F. Absorption by Gas in Presence of a Magnetic Field

A travelling wave linear accelerator usually consists of a high frequency power source feeding power into a waveguide accelerating tube which is terminated by a dummy load to absorb without reflection the power reaching the output end. It has been shown (Harvie 1948) that there is an optimum length of accelerating tube, which corresponds to an attenuation of approximately 1·25 nepers, but unfortunately there are sometimes practical difficulties in making accelerators as long as the optimum length. This note describes means for overcoming some of these difficulties, in which an accelerator of less than optimum length retains its efficiency by utilizing the power which is usually wasted in the dummy load.

The system is shown diagrammatically in Figure 1, in which arrows indicate the direction of power flow. Power is fed back from the output end of the accelerator and combined with the power from the source in a suitable bridge circuit. It is sometimes

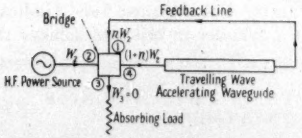

Figure 1. Diagrammatic arrangement of linear accelerator with feedback.

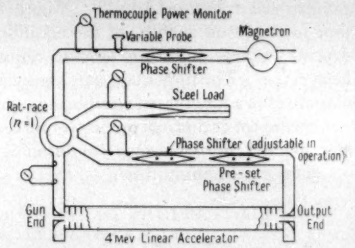

Figure 2. Feedback system applied to 4 MEV. linear accelerator.

desirable that arms (1) and (2) of the bridge should be mutually conjugate, in order to make the impedance presented to the source constant during a transient building-up period and independent of the accelerator characteristics. It can then be shown that the bridge circuit must include a dissipative element which is shown connected to arm (3) externally; under steady state conditions no power is dissipated in this element. Steady state power fluxes are shown on the diagram; the power flux entering the accelerator $(1+n)W_2'$ is always greater than the power supplied by the source and n is determined by the attenuation of the accelerator. Calculations show that the "efficiency" of the accelerator, V^2/WL, increases as the length is diminished and is slightly greater than that of an optimum length accelerator with a dummy load at the end.

Bridges of the type required have been studied previously (Tyrell 1947, Smullin and Montgomery 1948) for the special case where $n=1$, and examples will be familiar under the names of "magic T" and "Rat-race". There seems to be no great difficulty in designing bridges along similar lines for other values of n.

In a pulse operated system it is necessary for waves to make several transits of the accelerator and feedback loop, after application of the pulse, before steady state conditions are approached. Calculations show that the build-up time is independent of the length and is approximately the same as in a conventional accelerator of optimum length. If the frequency of the source is varied the power fed back from the end does not return in the correct phase and the circulating power is reduced. It can be shown that the permissible frequency bandwidth is again approximately the same as in an ordinary accelerator of

optimum length; however, by adding an adjustable phase changer in the feedback path it is possible to maintain the correct circulating power at any frequency and the bandwidth is then only limited by the wave-to-electron phasing in the usual way.

An advantage of the system is that the accelerator can be made appreciably shorter than the optimum length without losing efficiency, which leads to increased dimensional tolerances on the waveguide. A shorter waveguide also has a wider frequency bandwidth, as far as phasing of the wave to electrons is concerned, and it may also be an advantage in practice to allow the frequency of the source to vary as it will within this band while the operating conditions are kept right by adjusting the phase changer in the feedback loop.

For the case of a bridge circuit designed for $n=1$, theoretical curves can be plotted for the power in the various arms of the bridge when the phase and attenuation in the accelerator loop are varied. Experimental confirmation has been obtained at low C.W. power with a mock-up system on a wavelength of 3·2 cm., using a normal $n=1$ " Rat-race " and about 30 wavelengths of rectangular waveguide to represent in some measure the corrugated waveguide. A method has also been worked out theoretically and confirmed experimentally for obtaining a suitable signal which will reset the phase shifter in the feedback arm when the magnetron frequency changes.

It has also been possible to try out the $n=1$ system on the 4 MeV. linear accelerator (Fry *et al.* 1948) since the R.F. loss in the accelerator is about 2·5 db. and can be made up to 3 db. with beam loading. The experiment had unfortunately to be carried out in a very short time and the external waveguide components were not matched as well as they should have been; consequently the thermocouple power monitors could not be relied upon to within 20%, although they were partly compensated for by the presence of standing waves. It was not therefore possible to verify the power fluxes in all parts of the system. However, independent measurements showed that the accelerator operated as if it had an input R.F. power flux of 2·1–2·2 MW. when the magnetron power was only about 1·4 MW. The energy spectrum was identical to that previously obtained with the same input power but without feedback. The maximum power which could be obtained in the accelerator was 2·4 MW. and, with a somewhat lower frequency than normal, the mean energy was raised to 4·5 MeV. but with more than twice the normal spectrum width. These experiments indicated that a well matched system would work as predicted, but with one reservation—that a somewhat better vacuum is required than for an equivalent accelerator without feedback.

It was noticed that the loss in the corrugated waveguide soon after applying the R.F. power but without the gun in operation was very greatly increased when the focusing field was switched on, and moreover the effect happened quite critically at about one-third of the normal focusing field and was not confined to any particular spot along the length of the corrugated waveguide. It has been checked that the power leaving the accelerator falls in the same manner for the system without feedback, but since there is no reaction on the input power its effect on this particular accelerator is not serious and had therefore not been observed before. The effect may be due to the presence of positive ions or electrons which spiral under the influence of the focusing field and consequently abstract very much greater quantities of energy from the R.F. wave than if they drifted straight to the walls of the tube. As the vacuum cleans up the effect entirely disappears and the operation is as predicted.

This work was carried out as part of the programme of the Accelerator Group of the Atomic Energy Research Establishment at the Telecommunications Research Establishment, Malvern, and acknowledgment is made to the Director, A.E.R.E., for permission to publish the results.

Atomic Energy Research Establishment
at Telecommunications Research Establishment,
Malvern, Worcs.
3rd February 1949.

R. B. R.-SHERSBY-HARVIE.
L. B. MULLETT.

FRY, D. W., *et al.*, 1948, *Nature, Lond.*, **162**, 859.
HARVIE, R. B. R.-S.-, 1948, *Proc. Phys. Soc.*, **61**, 255.
SMULLIN, L. D., and MONTGOMERY, C. G., 1948, *Microwave Duplexers* (New York and London: McGraw Hill).
TYRELL, W. A., 1947, *Proc. Inst. Radio Engrs.*, **35**, 1294.

The Dielectric Properties of Ice at 1·25 cm. Wavelength

It is known that ice exhibits a loss-maximum dependent upon temperature, in the frequency range 10^4 to 10^5 c/s. (Granier 1924, Errera 1924, Smyth and Hitchcock 1932, Eder 1947): it has also been shown by Lamb (1946 a) that, at $-5°$ c., the resulting absorption is characterized by a single relaxation time. Lamb (1946 a) further measured the dielectric properties at a free space wavelength of 3 cm. over the temperature range 0 to $-50°$ c., using an H_{01} cylindrical cavity type of resonator. Under these conditions the permittivity was sensibly constant and was given as $3{\cdot}0_5$; further experience with the apparatus used in these experiments, however, has indicated that this value should be increased by approximately 4% owing to the use of a metal cup to contain the ice specimen within the resonator. The corrected permittivity value of $3{\cdot}1_7$ is appreciably greater than the square of the optical refractive index, $n^2=1{\cdot}72$ (International Critical Tables I, 166), and the measurements have now been extended to a free space wavelength, $\lambda=1{\cdot}25$ cm., and to temperatures as low as $-195°$ c., in an attempt to observe a second dispersion. An H_{01} cylindrical cavity resonator has also been used in these experiments (Lamb 1946 b), but in this case the ice specimen was formed to fit loosely in the cavity and rested on the movable piston. Each specimen was prepared from water which had been distilled once.

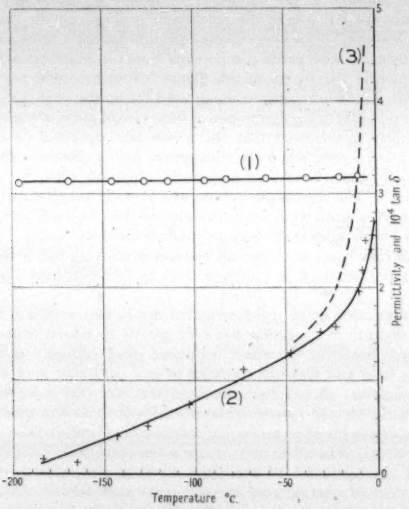

Curve 1. Measured permittivity values at $\lambda=1{\cdot}25$ cm., without correction for change in specimen thickness with temperature.
Curve 2. Measured tan δ values at $\lambda=1{\cdot}25$ cm
Curve 3. Tan δ-temperature curve for $\lambda=3$ cm. reproduced from Lamb's paper.

The results obtained are given in the Figure, in which the tan δ–temperature curve or $\lambda=3$ cm. is reproduced. At any given temperature the loss-factor value at $\lambda=1{\cdot}25$ cm. is slightly less than that at the higher wavelength, but its variation with temperature is of a similar form. No appreciable change in permittivity was observed over the temperature range covered by the experiments: the small decrease at lower temperatures shown in the Figure could be accounted for by the change in specimen thickness with temperature for which no correction was applied. The permittivity near 0° c. is 3·18 (±2%), in agreement with the corrected value for $\lambda=3$ cm.

A decrease in temperature would displace a dispersion due to dipole relaxation towards a region of longer wavelength. Since, however, there is no evidence of a decrease in permittivity (nor of an increase in tan δ) at $\lambda=1{\cdot}25$ cm., even for temperatures as low as $-195°$ C., it is unlikely that the difference between the measured permittivity and the square of the optical refractive index can be explained by a further dipole relaxation. The difference could be attributed to a dispersion caused by vibration of the molecule about its equilibrium position in the crystal lattice at a resonance frequency considerably greater than 24,000 Mc/s. ($\lambda=1{\cdot}25$ cm.): an alternative explanation would be a comparatively large "atomic" polarization. The contribution to permittivity at $\lambda=1{\cdot}25$ cm. arising from either of these latter effects would be sensibly independent of temperature.

One of the authors (A. T.) wishes to thank the British Electrical and Allied Industries Research Association by whom he was employed during the progress of this work.

Electrical Engineering Dept.,
Imperial College, London S.W. 7.
31st January 1949.

JOHN LAMB.
A. TURNEY.

EDER, F. X., 1947, *Funk und Ton*, **1**, 21.
ERRERA, J., 1924, *J. Phys. Radium*, **5**, 304.
GRANIER, J., 1924, *C.R. Acad. Sci., Paris*, **179**, 1314.
LAMB, J., 1946a, *Trans. Faraday Soc.*, **42** A, 239; 1946b, *J. Instn. Elec. Engrs.*, **93**, Pt. IIIA, 1447.
SMYTH, C. P., and HITCHCOCK, C. S., 1932, *J. Amer. Chem. Soc.*, **54**, 4631.

REVIEWS OF BOOKS

Dipole Moments, by R. J. W. LE FÈVRE. Pp. 117. Second Edition, revised and reset. (London: Methuen, 1948.) 5*s*.

Since the first appearance, ten years ago, of this excellent little book, the reviewer has consistently recommended it to and for honours students in chemistry. Seeing that the second edition differs hardly at all from the first, he will continue to do so. The only changes worthy of note are the following.

At the very beginning of the book there is a new short section on the relationship of dielectric constant to other properties. This contains a sketchy account of certain empirical relations, so ancient as to be of scant interest. The reviewer cannot help wondering whether this insertion was by request.

The very useful chapter on experimental methods of measurement has been made yet more useful by the inclusion of further practical information.

The chapter on molecular structure contains new data on several pairs of geometrical isomers which have been investigated by the author and collaborators. The author makes the interesting suggestion that the rate of inter-conversion of geometrical isomers in solution could be determined by measuring the dielectric constant.

The reviewer's only criticisms are directed not at this particular book, but against certain features common to the whole literature of this subject.

One does not *measure* a dipole moment. One measures dielectric constants and refractive indices. Then by unnecessarily cumbrous algebraic formulae one calculates a dipole moment.

If the dipole moment thus calculated is found to differ according to the solvent, the cause may well be neither solute–solute interaction nor solute–solvent interaction, but just the inaccuracy of Debye's approximations, whose main justification is the lack of any better. This inadequacy was realized and stated by Debye, but seems to be forgotten or ignored by the majority of those who use his formulae.

When Onsager developed an improved theory of the dielectric constant of pure liquids, he indicated briefly that the treatment might be extended to solutions, but no one has yet followed this lead. We still lack a satisfactory theory of the dielectric constant of liquid mixtures.

E. A. G.

Progress in the Theory of the Physical Properties of Glass, by J. M. STEVELS. Pp. xi+104. (New York, Amsterdam, London, Brussels: Elsevier Publishing Company, Inc., 1948.) 10*s*. net.

Theories of the physical properties of glasses were almost non-existent until the pioneer work of Zachariasen and of Warren during the eight years immediately before the war. The present book describes the advances made in Holland during the war mainly through the efforts of Stevels and his associates at the Philips Research Laboratory, Eindhoven. In his preface the author makes it clear that no attempt has been made to take into account all the American and British literature published since 1939, although some additions from these sources were made during the correction of the proofs.

The first chapter presents a general account of glass in the solid state based mainly on the experimental work of Warren and the ideas of Zachariasen, who stated rules for deciding which inorganic oxides should form glasses in cases where the structures of the corresponding crystalline forms are known. The author's claim that complete agreement with the Zachariasen theory is found is of doubtful accuracy; the Zachariasen theory should be regarded rather as an excellent guide to probable glass-forming substances, but not yet completely proved or entirely free from ambiguity.

A long chapter on the density of glass is based on the theory of Stevels that the volume of a block of glass containing one gram atom of oxygen ions is in many cases given by an empirical formula involving the number of oxygen ions divided by the number of network-forming ions (Si^{4+}, B^{3+} etc.) and a constant depending upon the nature of the network formers, but to a first approximation not upon the nature and the amount of the network modifiers (Na^{+}, Ca^{2+} etc.). The significance of the formula in relation to structure is discussed at length for silicate, borate, borosilicate, boroaluminate, phosphate and germanate glasses. The chapter forms an impressive example of the value of a semi-empirical attack on the physical properties in advancing our knowledge of glass structure, even though neither the formula nor the values of the constants can be derived theoretically.

Chapter 3 deals in a general way with the electrical conductivity of glasses and provides a derivation of the Rasch and Hinrichsen law. Chapter 4 discusses dielectric losses in glasses; the theoretical background provided is the recent one of Gevers and du Pré, together with a theory of the relation between loss angle and glass composition. The theories should stimulate further research, particularly on the losses at low temperatures and over greater ranges of frequency or glass composition.

The fifth chapter deals with molecular refraction, the refraction being regarded as the sum of the contribution of each ionic constituent. The theory is restricted to certain ranges of composition only and, although the ionic refractivity of silicon is taken from the previous work of Fajans and Joos, the values for the oxygen, sodium, calcium and potassium ions are adapted to fit the experimental results.

It is easy to be critical of newly developed theories, and in the case of glass particularly so, in that so little sound theoretical work has been done in spite of a great number of technological measurements of physical properties. Dr. Stevels is to be congratulated therefore on his efforts to develop the theoretical aspects of glass physics. The book deserves careful study by all interested in glass science, and will serve its purpose if the limitations of the theories he puts forward stimulate further investigation.

J. E. STANWORTH.

CONTENTS FOR SECTION A

	PAGE
Dr. E. F. DALY and Dr. G. B. B. M. SUTHERLAND. The Performance of Infra-Red Spectrometers as Limited by Detector Characteristics	205
Mr. J. EWLES and Dr. G. C. FARNELL. The Luminescence of Wetted Solids	216
Mr. R. J. BRIGHT, Dr. D. A. JACKSON and Dr. H. KUHN. The Resolving Power and Intensity Relationships of the Fabry Perot Interferometer with Silvered Reflecting Surfaces	225
Miss M. E. PILLOW. Intensity Distribution for Bands of the γ-System of MgH^+	237
Dr. E. P. GEORGE and Mr. A. C. JASON. Nuclear Disintegrations in Photographic Plates exposed to Cosmic Rays under Lead Absorbers	243
Mr. D. E. BUNYAN, Dr. A. LUNDBY and Dr. D. WALKER. Experiments with the Delayed Coincidence Method, including a Search for Short-lived Nuclear Isomers	253
Discussion on paper by Dr. F. C. CHAMPION and Dr. R. R. ROY entitled "The Scattering of Fast β-Particles through Large Angles by Nitrogen Nuclei" (*Proc. Phys. Soc.*, 1948, **61**, 532)	264
Letters to the Editor:	
Mr. T. S. MOSS. Infra-Red Photoconductivity in Layers of Tellurium and Arsenic	264
Reviews of Books	266
Contents for Section B	267
Abstracts for Section B	267
Corrigenda	268

ABSTRACTS FOR SECTION A

The Performance of Infra-Red Spectrometers as Limited by Detector Characteristics, by E. F. DALY and G. B. B. M. SUTHERLAND.

ABSTRACT. The performance of the average infra-red spectrometer is conditioned mainly by the characteristics of the detector employed. Assuming a minimum usable energy level at the exit slit, the square of the minimum frequency band embraced by the exit slit is proportional to the minimum energy level and to the focal length of the collimator, and inversely proportional to the angular dispersion of the prism or grating, the area of the collimator mirror, the energy flux at the entrance slit and the slit length. If, however, the time of response of the detector is taken into account, the inter-relation of spectrum scanning speed, signal-to-noise ratio and resolving power must be considered. For this purpose a simplified model of an infra-red detector has been used, defined by three parameters. This allows the relative merits of detectors to be assessed and the performance of any given spectrometer with a specified detector to be estimated. The inter-relation of resolving power and spectral scanning speed has been examined for "chopped-beam" and "video" presentation.

The Luminescence of Wetted Solids, by J. EWLES and G. C. FARNELL.

ABSTRACT. An earlier observation that the association of a non-luminescent pure liquid with a non-luminescent solid produces fluorescence and phosphorescence in the liquid has been confirmed. The luminescent spectra of water, heavy water, and alcohols, as well as some other liquids with different negative radicals when adsorbed by various finely divided ionic solids have been examined and recorded. The positions of the maxima of the main broad band are very similar for all the hydroxy liquids even with different solids (band peaks in the range 4300–4500 A.) and are different for the same solid with liquids having different negative radicals. Preliminary experiments on the relation between brightness and relative amount of liquid indicate that the phenomena are associated with the active sites on the solid surface, and afford evidence of the existence of these and of their differences on the same solid.

Excitation spectra confirm preliminary observations that the adsorbed molecules have very abnormal absorption regions indicating considerable changes in energy levels. Two suggestions are made to explain the phenomena: (*a*) the energy changes may be correlated with the heat of adsorption on the active sites; (*b*) the adsorbed molecules are bonded to the solid by the positive radicals leaving an almost free negative ion.

The Resolving Power and Intensity Relationships of the Fabry Perot Interferometer with Silvered Reflecting Surfaces, by R. J. BRIGHT, D. A. JACKSON and H. KUHN.

ABSTRACT. By the use of a Fabry Perot etalon with very small spacing, the widths of the interference fringes were measured under conditions where the light could be considered as practically monochromatic. In this way, the resolving power which can be achieved with silver deposits of known optical density was determined for light of five different wavelengths between 6438 and 3610 A. The results can be used for selecting the most favourable thickness of silvering of etalon plates, namely that which gives the resolving power required for a given purpose without unnecessary loss of intensity. The application of the results to multiple etalons is discussed.

Intensity Distribution for Bands of the γ-System of MgH^+, by M. E. PILLOW.

ABSTRACT. The intensity distribution for bands of the γ-system of MgH^+ is deduced theoretically from the wave functions for the various energy states, and is compared with the distribution of the observed bands.

Lines of the (2,3) band, not previously noted, have been observed.

Nuclear Disintegrations in Photographic Plates exposed to Cosmic Rays under Lead Absorbers, by E. P. GEORGE and A. C. JASON.

ABSTRACT. Ilford Nuclear Research photographic plates have been exposed at the Jungfraujoch, altitude 3,457 metres, under lead screens of various thicknesses up to 28 cm. The intensity of the stars, and its variation with the number of tracks forming them, have been recorded for each thickness of absorber. The absorption curve of the star intensity shows that the range in lead of the radiation causing the stars is 310 ± 20 gm/cm². The size distribution is apparently the same under all absorbers.

The intensity and size distribution have also been recorded in similar plates exposed at sea level. The size distribution is again the same as that found for the high altitude plates, but the range in air of the primaries is 150 ± 7 gm/cm².

These results are consistent with the generally accepted view that the majority of the stars is caused by neutrons.

Experiments with the Delayed Coincidence Method, including a Search for Short-lived Nuclear Isomers, by D. E. BUNYAN, A. LUNDBY and D. WALKER.

ABSTRACT. The delayed coincidence method has been studied in some detail and employed in a search for short-lived isomers in the product nuclei of β-emitters. The influence of counter time-lag fluctuations, which determine the short half-life limit in this method, is discussed in relation to the " differential " procedure for recording the delayed coincidences. It is shown that the time lags exhibited by a Geiger-Müller counter are distributed approximately according to a Gaussian law. A differential delayed coincidence recorder has been constructed in which the overall time-lags in the two input channels due to " rise-time " effects have been stabilized. At the coincidence stage of this recorder the quadratic mean deviation in the time-lag difference between the two channels due to " rise-time " effects has been kept as low as $\sim 5 \times 10^{-9}$ sec. Details are given of the experimental procedure used in searching for short-lived isomers. The range of possible half-lives most thoroughly investigated extends from about 3×10^{-7} sec. to about 10^{-3} sec. for isomeric transitions giving conversion electron energies greater than about 100 kev. Possible improvements in the range of the experiments are discussed. The short-lived isomers of ^{181}Ta and ^{187}Re have been confirmed. The half-life of the metastable state in ^{187}Re has been found to be $(5{\cdot}26 \pm 0{\cdot}12) \times 10^{-7}$ sec. Negative results are reported for 19 isotopes. In particular the metastable states reported by other authors in ^{198}Hg, ^{141}Pr, and ^{124}Te are not confirmed.

The half-life of ThC′ has been found to be $(3{\cdot}04 \pm 0{\cdot}04) \times 10^{-7}$ sec.